Proceedings of the International School of Physics "Enrico Fermi"
Course 190 "Frontiers in Modern Optics", edited by D. Faccio, J. Dudley and M. Clerici
(IOS, Amsterdam; SIF, Bologna) 2016
DOI 10.3254/978-1-61499-647-7-31

Tutorial on nonlinear optics

S. Choudhary

School of Electrical Engineering and Computer Science, University of Ottawa
Ottawa, Ontario, K1N 6N5 Canada

R. W. Boyd

School of Electrical Engineering and Computer Science, University of Ottawa
Ottawa, Ontario, K1N 6N5 Canada

The Institute of Optics, University of Rochester
Rochester, New York, 14627 USA

Department of Physics, University of Ottawa
Ottawa, Ontario, K1N 6N5 Canada

Summary. — Nonlinear optics deals with phenomena that occur when a very intense light interacts with a material medium, modifying its optical properties. Shortly after the demonstration of first working laser in 1960 by Maiman (*Nature*, **187** (1960) 493), the field of nonlinear optics began with the observation of second harmonic by Franken *et al.* in 1961 (*Phys. Rev. Lett.*, **7** (1961) 118). Since then, the interest in this field has grown and various nonlinear optical effects are utilized for purposes such as nonlinear microscopy, switching, harmonic generation, parametric downconversion, filamentation, etc. We present here a brief overview of the various aspects on nonlinear optics and some of the recent advances in the field.

1. – Introduction to nonlinear optics

According¡proofsAuthor please note that we have written in full the reference quotations in the abstract and reordered those in the text accordingly, following the numerical sequence. Please check, thanks to ref. [1], nonlinear optics is the study of phenomena that occur due to the modification of material properties in the presence of light of high intensity. The nonlinearity is associated with the fact that material response varies in a nonlinear manner with the applied optical field. To study this effect, we consider the dependence of the dipole moment per unit volume, or polarization $\tilde{P}(t)$ on the applied optical field strength $\tilde{E}(t)$. On application of the optical field, there is displacement of both electrons and the nuclei with respect to the centre of mass of the molecule. Considering dipole approximation, an electric dipole is formed due to charge separation between the negatively charged electron cloud and the positively charged nucleus. At optical frequencies, due to its much larger mass, the oscillations in the nucleus are much weaker than the electronic oscillations. Hence the nuclear contributions are far weaker than the electronic contributions, at least for linear polarizability. The nonlinear susceptibility on the other hand (manifested in terms of Raman scattering), might be comparable or even larger depending on whether we are on or off resonance [2]. But for all practical purposes, we neglect the nuclear contributions for simplicity in our present discussion. The bulk polarization of the entire material is thus a vector sum of the dipole moments of all the molecules [3, 4]. In a linear regime, the induced dipole also oscillates with the same frequency as the driving field and each molecule of the material can be viewed as a harmonic oscillator.

Due to larger mass of the nucleus, these oscillations are very weak and about the mean position of the molecules. The induced polarization in this case can be expressed as

$$\tilde{P}(t) = \epsilon_0 \chi^{(1)} \tilde{E}(t), \tag{1}$$

where ϵ_0 is the permittivity of free space and the $\chi^{(1)}$ is the linear susceptibility.

But for larger applied fields (comparable to inter-atomic fields) and proportionately stronger oscillations, this approximation breaks down and the behaviour deviates from that of a harmonic oscillator. In this anharmonic case, nonlinear terms come into play which give rise to different frequency components in the oscillations. To account for this, we expand the polarization $\tilde{P}(t)$ as a generalized power series in $\tilde{E}(t)$ and include all the nonlinear contributions as

$$\begin{aligned} \tilde{P}(t) &= \epsilon_0 \left[\chi^{(1)} \tilde{E}^1(t) + \chi^{(2)} \tilde{E}^2(t) + \chi^{(3)} \tilde{E}^3(t) + \ldots \right], \\ \tilde{P}(t) &= \tilde{P}^1(t) + \tilde{P}^2(t) + \tilde{P}^3(t) + \ldots \ . \end{aligned} \tag{2}$$

The constants $\chi^{(2)}$ and $\chi^{(3)}$ are the second- and third-order nonlinear optical susceptibilities, respectively. This is a very simplified notation and does not take into account dispersion or losses because of the instantaneous nature of the response. Under general circumstances when losses and dispersion are present, the susceptibilities depend on frequency. If the vector nature of fields is also taken into account, then $\chi^{(1)}$ is a tensor of

rank 2, $\chi^{(2)}$ a tensor of rank 3 and so on. $\tilde{P}^1(t)$ is called the linear polarization while $\tilde{P}^2(t)$ and $\tilde{P}^3(t)$ are called the second- and third-order nonlinear polarizations respectively. Thus, the polarization is composed of linear and nonlinear components. A time varying nonlinear polarization is a source of newer electromagnetic field components and hence is key to the description of nonlinear optical phenomena. This is evident in the wave equation for nonlinear media:

$$\bigtriangledown^2\tilde{E} - \frac{n^2}{c^2}\frac{\partial^2\tilde{E}}{\partial t^2} = \frac{1}{\epsilon_0 c^2}\frac{\partial^2\tilde{P}^{\mathrm{NL}}}{\partial t^2}\,. \tag{3}$$

Here, the nonlinear polarization $\tilde{P}^{\mathrm{NL}}$ drives the electric field $\tilde{E}$ and the term $\partial^2\tilde{P}^{\mathrm{NL}}/\partial t^2$ represents the acceleration of charges in the medium. This is consistent with Larmor's theorem that accelerating charges generate electromagnetic waves. It should be noted that under certain circumstances such as resonant excitation of atomic systems or under very high applied laser field strength, the power series representation of (2) may not converge. Such cases are dealt with a formalism that includes the possibility of saturation effects.

Susceptibilities may be complex or real depending on whether the nonlinear process involves exchange of energy with the medium or not, respectively. When there is no energy exchange between the interacting waves and the medium and the quantum state of the medium remains unchanged in the end (there may be population transfers between real and virtual levels but they have a very short lifetime), the process is called a "parametric process". Examples include SHG, SFG, DFG, OPA, THG, Kerr nonlinearity, SPM, XPM, FWM, etc, using standard notation that will be developed within this chapter. When the quantum state of the medium is changed in the end, the process is called a non-parametric process. Examples include SRS, SBS, multi-photon absorption, saturable absorption, etc. A brief description of all these processes are provided in the sections that follow.

2. – Second-order nonlinear optical processes

The discovery of second-harmonic generation (SHG) in 1961 by Franken *et al.* [5] marked the beginning of the field of nonlinear optics. In 1965, ref. [6] reported the nonlinear light scattering in a quartz crystal generating light with frequency twice that of the incident beam. Difference-frequency generation by a KDP crystal using non-collinear light beams was also reported in 1965 in ref. [7]. Apart from second-harmonic generation, the effects that result from second-order nonlinearity or a non-zero $\chi^{(2)}$ include sum- and difference-frequency generation, optical parametric oscillation and spontaneous parametric downconversion. Material symmetry plays a significant role in determining the second-order response as only non-centrosymmetric materials, or materials lacking inversion symmetry show a second-order response. This will be elaborated later. A brief description of each of the second-order processes mentioned above is as follows.

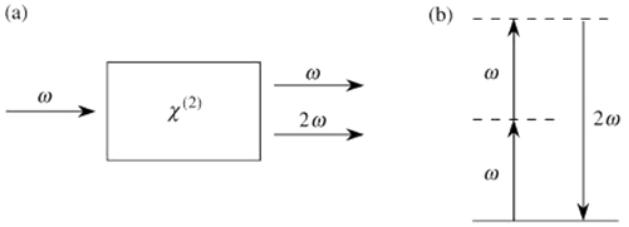

Fig. 1. – (a) Schematic showing SHG process. (b) Energy level diagram for SHG process.

2˙1. *Second-harmonic generation (SHG).* – When a monochromatic laser beam of electric field strength represented by

$$\tilde{E}(t) = Ee^{-i\omega t} + \text{c.c.} \tag{4}$$

is incident on a material with non-zero value of $\chi(2)$, it induces a second-order polarization given by

$$\begin{aligned} \tilde{P}^{(2)}(t) &= \epsilon_0 \chi(2) \left(Ee^{-i\omega t} + \text{c.c.}\right)^2, \\ \tilde{P}^{(2)}(t) &= \epsilon_0 \chi^{(2)} \left(2EE^* + E^2 e^{-2i\omega t} + E^{*2} e^{2i\omega t}\right), \\ \tilde{P}^{(2)}(t) &= 2\epsilon_0 \chi^{(2)} EE^* + \left(\epsilon_0 \chi^{(2)} E^2 e^{-2i\omega t} + \text{c.c.}\right). \end{aligned} \tag{5}$$

The second term oscillates with a frequency 2ω and is the second-harmonic contribution to the polarization, while the constant first term represents a static electric polarization developed in the material (as $\partial^2 \tilde{P}^{\text{NL}}/\partial t^2$ vanishes) and is called the optical rectification term. So we see that the second-harmonic term scales quadratically with the incident electric field. It is to be noted though that $\chi^{(2)}$ has an order of magnitude value of approximately 10^{-12} m/V, and one might thus think that this contribution is not significant. But with proper experimental conditions, very high efficiencies can be obtained such that nearly all the incident power is converted into the second harmonic.

Figure 1b shows an energy level diagram of the SHG process. The solid line indicates the ground state while the dotted lines indicate virtual levels. This diagram illustrates that two photons of frequency ω are annihilated and one photon of frequency 2ω is created. Some results of a laboratory demonstration of SHG are shown in fig. 2.

2˙1.1. Mathematical description. The mathematical treatment provided here follows those discussed in refs. [4, 1] and [9]. To develop a mathematical description of SHG, we need to derive the coupled wave equations for the incident pump field and the generated second-harmonic field within the material. We assume that the medium is lossless at the fundamental frequency ω_1 as well as the second-harmonic frequency $\omega_2 = 2\omega_1$ and that the input beams are collimated, monochromatic and continuous-wave. The total electric

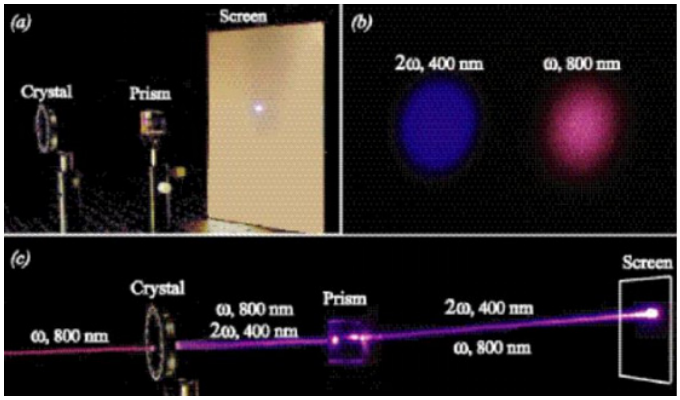

Fig. 2. – SHG from lithium niobate crystal. (a) Setup, (b) Screen output. (c) Trajectories of the pump and the SHG [8].

field within the nonlinear medium is given by

$$\tilde{E}(z,t) = \tilde{E}_1(z,t) + \tilde{E}_2(z,t), \tag{6}$$

where

$$\tilde{E}_j(z,t) = E_j(z)e^{-i\omega_j t} + \text{c.c.}, \qquad E_j(z) = A_j(z)e^{ik_j z} \tag{7}$$

with $k_j = n_j\omega_j/c$ and $n_j = [\epsilon^{(1)}(\omega_j)]^{1/2}$.

The amplitude of the second-harmonic wave $A_2(z)$ is taken to be a slowly varying function of z when the nonlinear source term is not too large, in the absence of which A_2 is constant (as it should be for a plane-wave solution). The nonlinear polarization is

$$\tilde{P}^{\text{NL}}(z,t) = \tilde{P}_1(z,t) + \tilde{P}_2(z,t), \tag{8}$$

where

$$\tilde{P}_j(z,t) = P_j(z)e^{-i\omega_j t} + \text{c.c.}, \quad j = 1,2 \tag{9}$$

and

$$P_2(z) = \epsilon_0\chi^{(2)}E_1(z)^2 = \epsilon_0\chi^{(2)}A_1^2e^{2ik_1 z}. \tag{10}$$

As each frequency component obeys the inhomogeneous wave equation (3), we can write the wave equation for the second harmonic as

$$\bigtriangledown^2\tilde{E}_2 - \frac{{n_2}^2}{c^2}\frac{\partial^2\tilde{E}_2}{\partial t^2} = \frac{1}{\epsilon_0 c^2}\frac{\partial^2\tilde{P}^2}{\partial t^2}\,. \tag{11}$$

On expanding the first term and rewriting the equation, we get

$$\left[\frac{\partial^2 A_2}{\partial z^2} + 2ik_2\frac{\partial A_2}{\partial z} - {k_2}^2 A_2 - \frac{{n_2}^2{\omega_2}^2}{c^2}\frac{\partial^2 A_2}{\partial t^2}\right] e^{i(k_2 z-\omega_2 t)} = -\frac{{\omega_2}^2}{c^2}\chi^{(2)}{A_1}^2 e^{2ik_1 z-\omega_2 t}. \tag{12}$$

We take the slowly varying amplitude approximation which allows us to neglect the first term as it is much smaller than the second. Also, using ${k_2}^2 = {n_2}^2{\omega_2}^2/c^2$, we get

$$2ik_2\frac{\partial A_2}{\partial z} = -\frac{\omega_2^2}{c^2}\chi^{(2)}{A_1}^2 e^{i\Delta kz}, \tag{13}$$

where $\Delta k = 2k_1 - k_2$ is known as the phase or wave vector mismatch factor and is crucial in determining the efficiency of the conversion process. It accounts for the conservation of momentum for the SHG process when we consider the quantum mechanical picture.

For simplicity, we make the undepleted pump approximation which means that $A_1(z)$ is taken to be constant. It is a valid approximation in most cases as at most a negligible fraction of the pump power is transferred to the generated fields. This simplifies the expression even further and we obtain

$$2ik_2\frac{\mathrm{d}A_2}{\mathrm{d}z} = -\frac{{\omega_2}^2}{c^2}\chi^{(2)}{A_1}^2 e^{i\Delta kz} = -\frac{4{\omega_1}^2}{c^2}\chi^{(2)}{A_1}^2 e^{i\Delta kz}. \tag{14}$$

On integrating both sides over the length L of the medium, we obtain

$$A_2(L) = \frac{2\omega_1}{n_2 c}\chi^{(2)}\,\frac{e^{i\Delta kL}-1}{\Delta k}\,. \tag{15}$$

For the case of perfect phase-matching or $\Delta k = 0$, on taking the limit $\Delta k \to 0$ in the above equation, we find

$$A_2(L) = \frac{2i\omega_1}{n_2 c}\chi^{(2)}{A_1}^2 L. \tag{16}$$

The intensity is given by $I_2 = 2n_2\epsilon_0 c|A_2(L)|^2$, where

$$|A_2(L)|^2 = \frac{4{\omega_1}^2}{{n_2}^2 c^2}\left[\chi^{(2)}\right]^2 |A_1|^4 L^2. \tag{17}$$

So the SHG intensity scales quadratically with the length of the medium or crystal. For the more general case of a nonzero Δk, we find

$$|A_2(L)|^2 = \frac{4{\omega_1}^2}{{n_2}^2 c^2}\left(\chi^{(2)}\right)^2 |A_1|^4 L^2\,\mathrm{sinc}^2\left(\frac{\Delta kL}{2}\right). \tag{18}$$

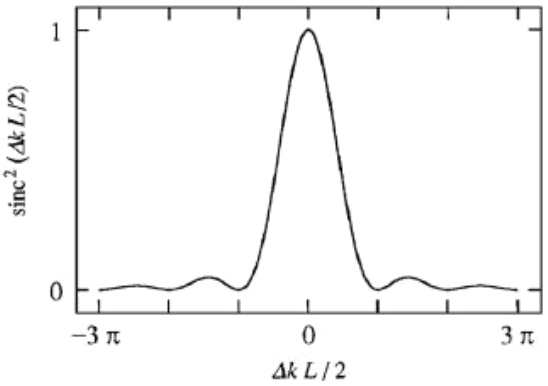

Fig. 3. – Intensity of the second-harmonic wave *versus* wave vector mismatch.

In this case, the intensity of the second-harmonic wave varies with the phase mismatch ΔkL as $[\mathrm{sinc}^2(\Delta kL/2)]$ as shown in fig. 3.

The coherence length is defined as the distance at which the output goes out of phase with the pump wave and is given by

$$L_{\mathrm{coh}} = \frac{2}{\Delta k}\,. \tag{19}$$

2˙2. *Sum frequency generation (SFG).* – Sum frequency generation is a more general situation than SHG in that the two input pump beams have different frequencies ω_1 and ω_2, leading to the generation of the sum frequency $\omega_3 = \omega_1 + \omega_2$. The total electric field associated with the input waves is given by

$$\tilde{E}(t) = E_1 e^{-i\omega_1 t} + E_2 e^{-i\omega_2 t} + \mathrm{c.c.} \tag{20}$$

The second-order nonlinear polarization in this case is given by

$$\tilde{P}^{(2)}(t) = \epsilon_0 \chi^{(2)} \tilde{E}(t)^2 \tag{21}$$

which on substitution of the expression for electric field gives

$$\begin{aligned}\tilde{P}^{(2)}(t) = \epsilon_0 \chi^{(2)} \Big[&{E_1}^2 e^{-2i\omega_1 t} + {E_2}^2 e^{-2i\omega_2 t} + 2E_1 E_2 e^{-i(\omega_1+\omega_2)t} \\ &+ 2E_1 {E_2}^* e^{-i(\omega_1-\omega_2)t} + \mathrm{c.c.}\Big] + 2\epsilon_0 \chi^{(2)} \left[E_1 {E_1}^* + E_2 {E_2}^*\right].\end{aligned} \tag{22}$$

The polarization $\tilde{P}^{(2)}(t)$ can be expanded in its Fourier series and the corresponding frequency components on both sides are equated to get the complex amplitudes of different

frequency components of the nonlinear polarization

$$
\begin{aligned}
P(2\omega_1) &= \epsilon_0 \chi^{(2)} {E_1}^2; \quad \text{(SHG)},\\
P(2\omega_2) &= \epsilon_0 \chi^{(2)} {E_2}^2; \quad \text{(SHG)},\\
P(\omega_1+\omega_2) &= 2\epsilon_0 \chi^{(2)} E_1 E_2; \quad \text{(SFG)},\\
P(\omega_1-\omega_2) &= 2\epsilon_0 \chi^{(2)} E_1 {E_2}^*; \quad \text{(DFG)},\\
P(0) &= 2\epsilon_0 \chi^{(2)} \left[E_1 {E_1}^* + E_2 {E_2}^*\right]; \quad \text{(OR)}.
\end{aligned} \tag{23}
$$

As we can see from the above equations, in the most general case of mixing between two pump beams, we get second harmonic (SHG), sum frequency (SFG), difference frequency (DFG) and optical rectification (OR). But all these components are not present at the same time and it is mostly one component that is the dominant one which is determined by the phase-matching condition (to be discussed later).

2˙2.1. Mathematical description. The derivation of the coupled wave equations is similar to that of second-harmonic generation except for the nonlinear source term which in the case of two pump beams becomes

$$
\tilde{P}_3(z,t) = P_3(z) e^{-i\omega_3 t}, \quad \text{where} \quad P_3(z) = 2\epsilon_0 \chi^{(2)} A_1 A_2 e^{-i(k_1+k_2)z}. \tag{24}
$$

Also,

$$
\tilde{E}_3(z,t) = A_3(z) e^{i(k_3 z - \omega_3 t)} + \text{c.c.}, \quad \omega_3 = \omega_1 + \omega_2, \tag{25}
$$

where

$$
k_3 = \frac{n_3 \omega_3}{c}, \quad {n_3}^2 = \epsilon^{(1)}(\omega_3). \tag{26}
$$

Note that the complex envelope $A_3(z)$ is again a slowly varying function of z in the presence of a small nonlinear source term which would have otherwise been a constant leading to a uniform plane-wave solution. Also, we make the undepleted pump approximation for both A_1 and A_2 and take them as constants in the analysis. As each frequency component of the electric field satisfies the inhomogeneous wave equation, we write the wave equation for the sum frequency term

$$
\begin{aligned}
&\left[\frac{\partial^2 A_3}{\partial z^2} + 2ik_3 \frac{\partial A_3}{\partial z} - {k_3}^2 A_3 - \frac{{n_3}^2 {\omega_3}^2}{c^2} \frac{\partial^2 A_3}{\partial t^2}\right] e^{i(k_3 z - \omega_3 t)}\\
&= -2\frac{{\omega_3}^2}{c^2} \chi^{(2)} A_1 A_2 e^{i(k_1+k_2)z - \omega_3 t}
\end{aligned} \tag{27}
$$

Again, making the slowly varying envelope approximation and substituting the value of $k_3 = n_3\omega_3/c$, we obtain

$$
\frac{\mathrm{d}A_3}{\mathrm{d}z} = \frac{i\chi^{(2)} {\omega_3}^2}{k_3 c^2} A_1 A_2 e^{i\Delta k z}, \tag{28}
$$

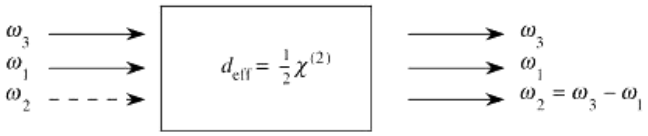

Fig. 4. – Schematic showing the process of difference frequency generation.

where $\Delta k = k_1 + k_2 - k_3$ is the phase or wave vector mismatch factor. Integrating the above equation along the length L of the crystal, we obtain

$$A_3(L) = \frac{i\chi^{(2)}\omega_3 A_1 A_2}{n_3 c}\,\frac{e^{i\Delta kL} - 1}{i\Delta k}\,. \tag{29}$$

The intensity of the sum frequency wave at the output of the crystal is given by $I_3(L) = 2n_3\epsilon_0 c|A_3(L)|^2$ where

$$|A_3(L)|^2 = \frac{2{\chi^{(2)}}^2\omega_3{}^2 I_1 I_2}{n_1 n_2 n_3 \epsilon_0 c^2} L^2\,\mathrm{sinc}^2\left(\frac{\Delta kL}{2}\right). \tag{30}$$

So the sum-frequency intensity also shows a sinc^2 dependence, as was observed for the second-harmonic case. Figure 3 thus also shows the variation of sum frequency intensity as a function of the phase mismatch factor.

2˙3. *Difference Frequency Generation (DFG).* – In the previous section, we saw that a difference frequency component was one of the outcomes when two beams interact in a medium with non-zero value of $\chi^{(2)}$. Let us now consider in detail such a situation, which as shown in fig. 4, where two waves ω_3 and ω_1 interact in a lossless optical medium.

We use the undepleted pump approximation for the higher-frequency input wave ω_3. The coupled wave equations for the difference frequency wave ω_2 and the lower-frequency input wave ω_1 are obtained by a method analogous to that for SFG and are as follows:

$$\frac{\mathrm{d}A_1}{\mathrm{d}z} = \frac{i{\omega_1}^2\chi^{(2)}}{k_1 c^2} A_3 {A_2}^* e^{i\Delta kz}, \tag{31}$$

and

$$\frac{\mathrm{d}A_2}{\mathrm{d}z} = \frac{i{\omega_2}^2\chi^{(2)}}{k_2 c^2} A_3 {A_2}^* e^{i\Delta kz}, \tag{32}$$

where

$$\Delta k = k_3 - k_1 - k_2. \tag{33}$$

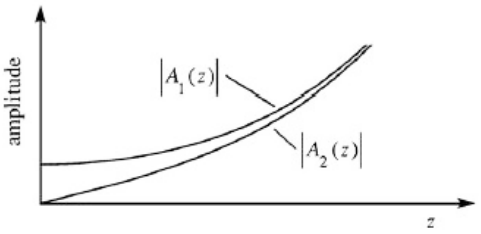

Fig. 5. – Spatial evolution of A_1 and A_2 for the case of perfect phase-matching in the undepleted pump approximation.

On solving the above set of differential equations for the case of perfect phase-matching, $\Delta k = 0$, we obtain

$$A_1(z) = A_1(0)\cosh \kappa z, \tag{34}$$

$$A_2(z) = i\left(\frac{n_1\omega_2}{n_2\omega_1}\right)^{1/2} \frac{A_3}{|A_3|} A_1{}^*(0)\sinh \kappa z, \tag{35}$$

where the coupling constant is given by

$$\kappa^2 = \frac{{\chi^{(2)}}^2 {\omega_1}^2 {\omega_2}^2}{k_1 k_2 c^4}|A_3|^2. \tag{36}$$

Figure 5 shows the spatial evolution of A_1 and A_2 for the case of perfect phase-matching in the undepleted pump approximation.

It is observed that both A_1 and A_2 show monotonically increasing growth and that each field asymptotically experiences an exponential growth. The input field A_1 retains its initial phase and the DFG wave A_2 possesses a phase that depends on both that of the pump and of the ω_1 waves. An intuitive explanation for this behavior is that the presence of the ω_2 wave stimulates the generation of the ω_1 wave and vice versa. This process of amplification of the signal wave ω_1 due to nonlinear mixing resulting in the production of an idler is known as "parametric amplification" as DFG is a parametric process (due to the initial and final quantum-mechanical states being identical).

2˙4. *Optical parametric oscillation (OPO).* – The previous section described the process of parametric amplification by DFG. This gain can be used to produce oscillation when it is supplied with the appropriate positive feedback. This can be done by placing mirrors that are highly reflective at one or both of the signal and idler frequencies on either side of the nonlinear medium as shown in fig. 6. If the end mirrors are reflecting at both the signal and idler frequencies, the device is called a doubly resonant oscillator, and if it is reflecting at either the signal or the idler frequency, then it is called singly resonant oscillator. The OPO can be used as a source of frequency-tunable radiation for

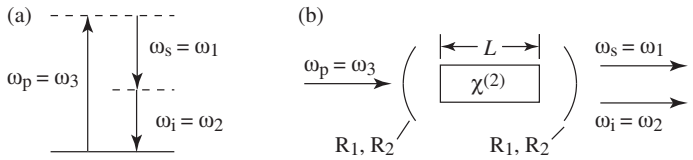

Fig. 6. – (a) Energy-level diagram for a parametric amplification process. (b) Schematic for an OPO.

infrared, visible and ultraviolet spectral regions and can produce either continuous wave, nanosecond, picosecond or femtosecond pulsed outputs.

2˙5. *Parametric downconversion.* – The production of simultaneous photon pairs was described as early as 1970 [10]. Also known as parametric fluorescence [11], parametric scattering or SPDC, it is the spontaneous splitting of the pump photon ω_p into signal, ω_s and idler, ω_p photons such that $\omega_p = \omega_s + \omega_i$ (energy conservation) and is stimulated by random vacuum fluctuations. The emitted photons must satisfy the phase-matching conditions due to momentum conservation, or $\vec{k_p} = \vec{k_s} + \vec{k_i}$.

The emitted photon pairs are simultaneously entangled in several sets of complementary degrees of freedom. Specifically, the photon pairs can be entangled in time and energy, in position and momentum, in orbital angular. The fact that the emitted photons display entanglement has enormous implications for quantum information technologies. For example, entanglement allows one to test some of the fundamental properties in quantum mechanics such reality and non-locality. SPDC is also used to build single photon sources. Entanglement between successive pairs does not occur [12]. Figure 7a shows the energy level diagram for this process and fig. 7b shows a typical experimental setup.

There are two different configurations for SPDC depending on whether the signal and idler waves have the same or orthogonal polarizations; these are called type-I and type-II configurations, respectively. For type I, the emission is in the form of concentric cones of signal and idler beams such that each photon of an entangled pair lie opposite to each other on the cones. In type II on the other hand, we get two separate cones for the orthogonal polarizations and each photon of the entangled pair is found opposite to each other on the respective cones. On the points of intersection of the two cones, we get photons that are entangled in polarization [13].

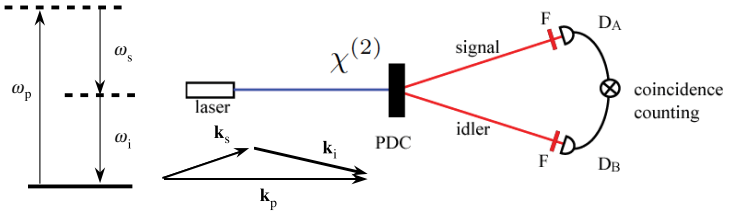

Fig. 7. – (a) Energy level diagram for a parametric downconversion process. (b) Schematic of an experiment to perform coincidence counts for entangled photons.

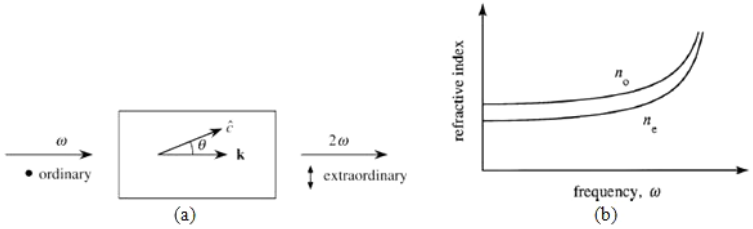

Fig. 8. – (a) Angle-tuned phase-matching. (b) Dispersion curves for a negative uniaxial crystal.

2˙6. *Phase-matching.* – In the previous sections, it was explained that the efficiency of all second-order processes depends on the crucial criterion of phase-matching. In vector representation, it is written as

$$\vec{k_1} = \vec{k_1} + \vec{k_3} \tag{37}$$

where $|\vec{k_i}| = n_i\omega_i/c$. When we consider collinearly propagating waves in an isotropic medium, this equation reduces to a scalar representation

$$\frac{n_1\omega_1}{c} = \frac{n_2\omega_2}{c} + \frac{n_3\omega_3}{c}\,. \tag{38}$$

From energy conservation, we have $\omega_1 = \omega_2 + \omega_3$. In a non-dispersive medium, we have $n_1 = n_2 = n_3$ and so eq. (37) is automatically satisfied in a non-dispersive medium due to frequency matching. But when we have a dispersive medium, the refractive indices are not equal (and increase monotonically with frequency) which means that both frequency and phase-matching conditions are not simultaneously satisfied and all the three waves travel with different velocities in the medium. As a result, we cannot have phase-matching in isotropic, dispersive media.

To compensate for the dispersion, birefringence, which is the dependence of refractive indices on polarization of the waves and the directions with respect to the principal axes of crystal, present in anisotropic media can be used. Hence, by properly adjusting the crystal orientation and the wave polarizations, phase-matching can be achieved. In [14], two ways of achieving phase-matching have been discussed: type I and type II. In type I, both lower frequency waves have ordinary polarization while in type II, one of them has the extraordinary polarization. Figure 8a shows how crystal angle can be tuned to achieve phase-matching in a negative uniaxial crystal.

In the case of a uniaxial crystal, we have further two possibilities depending on whether the ordinary refractive index or extraordinary refractive index is larger. Figure 8b shows the dispersion curve for a negative uniaxial crystal. Table I shows the phase-matching method for all four cases.

In cases where there is insufficient or no birefringence to compensate for dispersion, other methods need to be applied to achieve phase-matching. The most important

TABLE I. – *Phase-matching methods for uniaxial crystal.*

	Positive Uniaxial ($n_e > n_0$)	Negative Uniaxial ($n_e < n_0$)
Type I	${n_3}^o\omega_3 = {n_1}^e\omega_1 + {n_2}^e\omega_2$	${n_e}^o\omega_3 = {n_1}^o\omega_1 + {n_2}^o\omega_2$
Type II	${n_3}^o\omega_3 = {n_1}^o\omega_1 + {n_2}^e\omega_2$	${n_3}^e\omega_3 = {n_1}^e\omega_1 + {n_2}^o\omega_2$

method is called quasi–phase-matching where we have a periodically poled nonlinear crystal with the optic axis reversed at a period of less than or equal to twice the coherence length L_{coh} given by eq. (19). Hence every time the output goes out of phase with the pump causing power to flow back from the output, the sign of $\chi^{(2)}$ flips allowing the output to grow monotonically. Figure 9b shows the quasi–phase-matched output in comparison to perfectly phase-matched and phase-mismatched outputs.

3. – Third-order nonlinear optical processes

The third-order contribution to nonlinear polarization is given by

$$\tilde{P}^{(3)}(t) = \epsilon_0 \chi^{(3)} \tilde{E}(t)^3, \tag{39}$$

where $\tilde{E}(t)$ is the total electric field. The polarization then has various frequency components, the simplest being the third harmonic for the case of a monochromatic input.

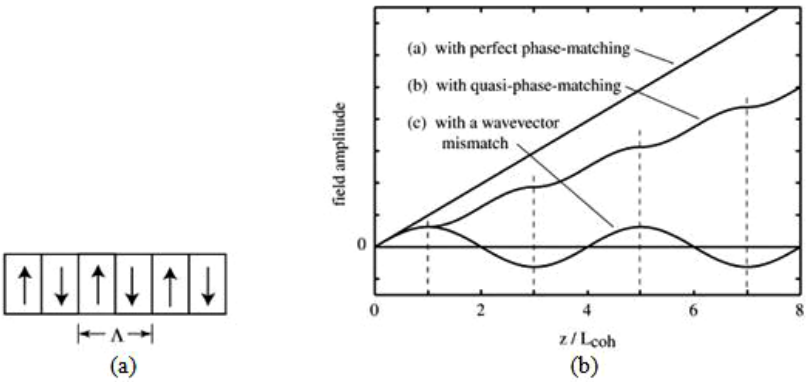

Fig. 9. – (a) A periodically poled crystal with arrows showing the direction of optic axis. (b) Comparison of perfect phase-matching and quasi–phase-matching.

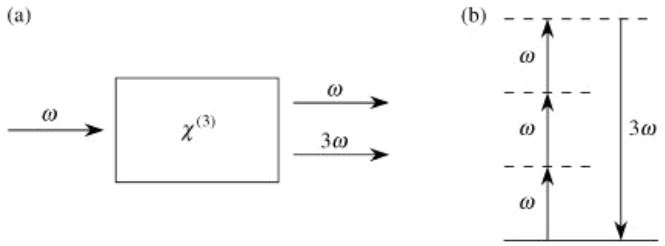

Fig. 10. – (a) Schematic for a THG process. (b) Energy level diagram for third-harmonic generation.

3˙1. *Third-harmonic Generation (THG).* – Let us consider the case of a monochromatic beam incident on the medium with the electric field given by

$$\tilde{E}(t) = Ee^{-i\omega t} + \text{c.c.} \tag{40}$$

The nonlinear polarization is then given by

$$\tilde{P}^{(3)}(t) = \epsilon_0 \chi^{(3)} \left[\left(E^3 e^{-3i\omega t} + \text{c.c} \right) + 3EE^* \left(E + E^* \right) e^{-i\omega t} \right] \tag{41}$$

The first term oscillating at frequency 3ω gives the third harmonic contribution. The energy level diagram for the process is shown in fig. 10.

3˙2. *Intensity dependent refractive index.* – In eq. (41), the second term oscillating at the frequency of the pump ω has the coefficient which depends on the intensity of the pump. So this contribution leads to a refractive index which depends on the intensity of the pump and is given by

$$n = n_0 + n_2 I. \tag{42}$$

It is also called the Kerr nonlinearity.

There are two ways in which this nonlinear effect becomes manifest: 1) Self-Phase Modulation (SPM): When a strong pump beam modifies its own propagation and 2) Cross-Phase Modulation (XPM): When a strong beam modifies the propagation of a weaker probe beam. Due to degeneracy factors associated with the coefficients, the nonlinear refractive index due to two beams, $\bar{n_2}^{\text{cross}}$, is twice that for a single beam, $\bar{n_2}^{\text{self}}$. By using the relation between the refractive index and susceptibility:

$$n_2 = 1 + \chi_{\text{eff}}, \tag{43}$$

where $\chi_{\text{eff}} = \chi^{(1)} + 3\chi^{(3)}|E|^2$, we find that

$$n_2 = \frac{3}{4{n_0}^2 \epsilon_0 c} \chi^{(3)} \tag{44}$$

for the case of SPM.

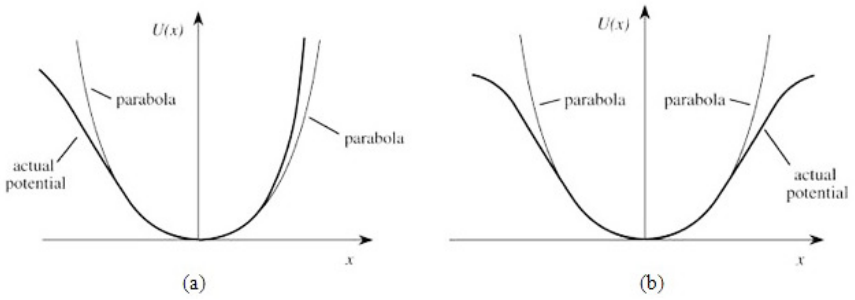

Fig. 11. – (a) Potential well for a non-centrosymmetric medium (b) Potential well for a centrosymmetric medium.

4. – Effect of material symmetry

Material symmetry, most importantly the presence of inversion symmetry, plays a very important role in determining the value of susceptibility. All even-order nonlinear responses vanishes identically for centrosymmetric materials, that is, for materials that lack inversion symmetry. Conversely, odd-order nonlinear response is in principle present for all materials. Figures 11a and b show the potential wells that confine electrons to their parent atom for centrosymmetric and non-centrosymmetric materials.

An intuitive explanation for this effect can be explained by examination of fig. 12, that shows the response for linear, centrosymmetric, and non-centrosymmetric media for a single-frequency applied field. While the response of a linear medium has the same form as the applied field with no distortion, the nonlinear responses for both types of nonlinear media shows significant distortion. For centrosymmetric media with potential well as shown in fig. 12a, only odd-harmonics are present in the response. For non-centrosymmetric media with potential well as shown in fig. 12b, both odd and even harmonics are present. Hence, we get a second-order nonlinear response from only non-centrosymmetric materials.

5. – Nonlinear optics with focussed Gaussian beams

The preceding sections have assumed infinite plane-wave sources for the description on nonlinear effects. But in actual practice, we do not have infinite plane waves. The laser beam typically is a Gaussian, and in this case we need to account for focussing effects including that the effective interaction length is the Rayleigh range of the beam. SHG using focussed Gaussian beams have been discussed in [15, 16] and [17].

For a Gaussian beam with waist diameter w_0, the Rayleigh range is

$$z_R = \frac{\pi {w_0}^2}{\lambda} \tag{45}$$

and the peak intensity $P/(\pi {w_0}^2)$ occurs the waist The peak intensity is thus inversely

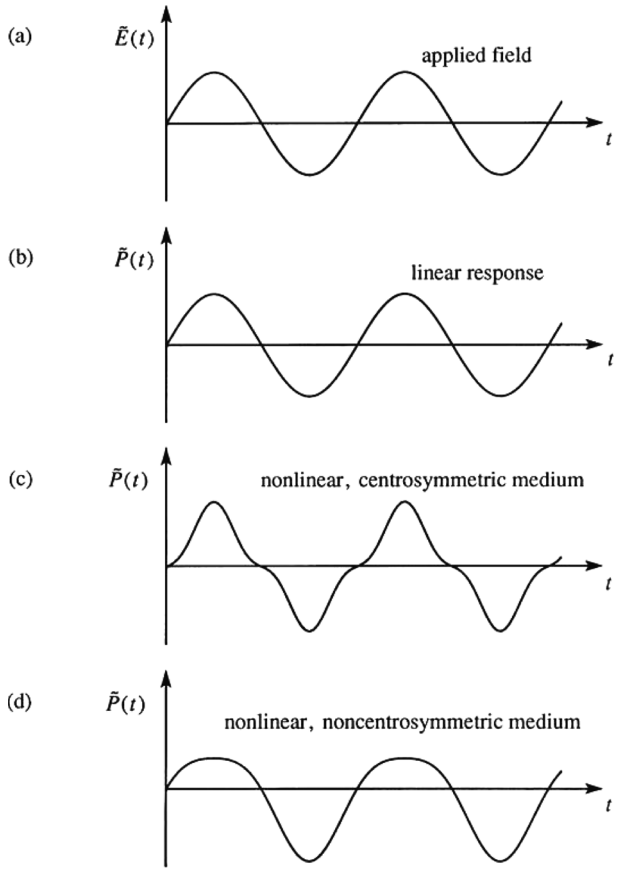

Fig. 12. – Response of centrosymmetric or non-centrosymmetric media to a plane wave excitation.

proportional to the length of the interaction region. So for maximum efficiency, the Rayleigh range must be half the length of the medium. But ref. [18] gives a value of $L/2.84$ for the confocal parameter (which is twice the Rayleigh range) for maximum efficiency of SHG. This is because we have an additional phase mismatch of $\Delta k = 3.2/L$ due to the Guoy phase shift which needs to be compensated.

6. – Origin of third-order nonlinear response

The nonlinear susceptibility is a characteristic of any given medium, and its value depends on the electronic and molecular structure of the material [9]. There are different mechanisms responsible for introducing an intensity-dependent refractive index, and their relative strengths and response times are summarized in table II.

Of the effects mentioned, the electronic polarizability is responsible for the generation of optical harmonics and has the fastest response. In liquids, effects due to molecular

TABLE II. – *Typical values of nonlinear refractive index (for linearly polarized light).*

Mechanism	n_2 (cm^2/W)	$\chi^{(3)}$ (m^2/V^2)	Response time (s)
Electronic polarization	10^{-16}	10^{-22}	10^{-15}
Molecular orientation	10^{-14}	10^{-20}	10^{-12}
Electrostiction	10^{-14}	10^{-20}	10^{-9}
Saturated atomic absorption	10^{-10}	10^{-16}	10^{-8}
Thermal effects	10^{-6}	10^{-12}	10^{-3}
Photorefractive effect	(large)	(large)	(intensity-dependent)

orientation and electrostriction dominate. Moreover, in solids with no degree of freedom for molecular orientation, electrostriction dominates.

6˙1. *Quantum-mechanical explanation of nonlinear optical susceptibility.* – The parametric nonlinear processes described in previous sections can be interpreted as a form of wave mixing involving energy exchange among the interacting waves of different frequencies. From a quantum mechanical perspective, they can be viewed as photon interaction processes involving creation of photons of some frequency and annihilation of another. This is represented in the energy-level diagrams illustrated previously. Thus, it involves electron transitions between the different energy levels which may be resonant, if they occur between real energy levels, or non-resonant, if they occur between virtual levels. Resonant transitions leads to a very large value of the susceptibility. The density-matrix formalism is the preferred means to derive expressions for the different orders of the nonlinear susceptibility $\chi^{(n)}$. A perturbation expansion is used to determine the expectation value of the induced dipole moment [9, 1]. Figure 13 shows the expression and Feynman diagrams [19, 1] for the each element of $\chi^{(2)}$, which represents a three photon interaction process.

6˙2. *Non-resonant electronic nonlinearities.* – Non-resonant nonlinearities arise due to electronic transitions involving virtual levels [1] and are the weakest of all contributions due to their off-resonance nature [1]. But these contributions are important as they are present in all dielectric materials. They are also extremely fast with response times of the order of 10^{-16} s, as the response time in this case is the time required for the atomic cloud to become distorted due to an applied optical field. We can estimate the order of magnitude of $\chi^{(3)}$ in the far-off resonance case by considering the classical, anharmonic model for an oscillator under far-off resonance excitation. The expression obtained is

$$\chi^{(3)} = \frac{Ne^4}{\epsilon_0 m^3 {\omega_0}^6 d^2}\,. \tag{46}$$

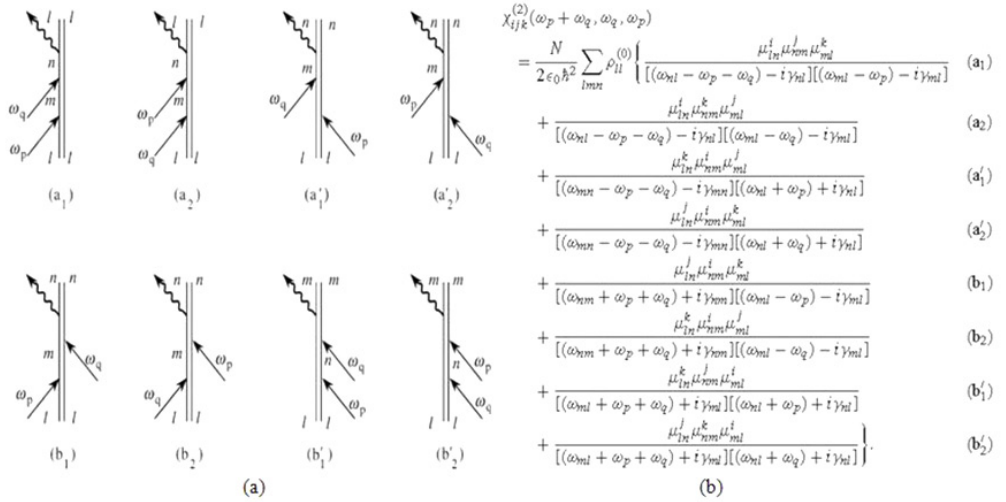

Fig. 13. – (a) Feynman diagrams for the electron transitions involved in a second-order process. (b) Expression for $\chi^{(2)}$ in terms of the transition dipole moments of the different transitions involved.

For the typical values of $N = 4 \times 10^{22}\,\mathrm{cm}^{-3}$, $d = 3 \times 10^{-10}\,\mathrm{m}$, and $\omega_0 = 7 \times 10^{15}\,\mathrm{rad/s}$ one finds that $\chi^{(3)} \simeq 3 \times 10^{-22}\,\mathrm{m}^2/\mathrm{V}^2$.

6˙3. *Molecular orientation effect.* – Molecular orientation contribution to the third order nonlinearity becomes important for anisotropic liquids *i.e.* liquids which have different polarizability along different axes. When subjected to an optical field, the molecules experience a torque that twists them such that the axis with higher polarizability tends to be aligned along the direction of the applied field. An example of such a liquid is carbon disulfide (CS_2), which is comprised of cigar-shaped (prolate spheroidal) molecule [1].

The polarizability along the molecular axis, α_3 is higher than along the transverse axis, α_1. Due to this, the induced dipole moment has a much larger component along the molecular axis than along the transverse axis and is not parallel to the applied field as shown in fig. 14. A net torque then acts on the molecule given by $\vec{\tau} = \vec{p} \times \vec{E}$ which tends to align the molecule with the applied electric field. But thermal agitation introduces a randomness in the molecular orientation. For a number density N temperature T, and neglecting the local-field effects, the first- and third-order susceptibilities for the given polarizabilities are given by

$$\chi^{(1)} = N\left(\frac{1}{3}\alpha_3 + \frac{2}{3}\alpha_1\right), \tag{47}$$

$$\chi^{(1)} = \frac{2N}{45}\frac{(\alpha_3 - \alpha_1)^2}{kT}, \tag{48}$$

where k is the Boltzmann constant. The response for this effect is slower as it takes some

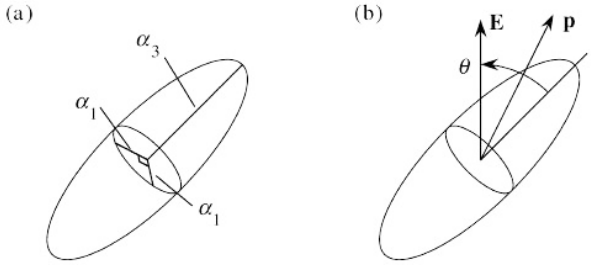

Fig. 14. – (a) The CS_2 molecule. (b) Dipole moments that develop within the molecule upon application of an electric field.

time for the molecules to align with the applied field, and the response time is of the order of picoseconds.

6˙4. *Thermal effects*. – Thermal contributions to the nonlinearity occur when the incident laser power when passing through them medium is absorbed causing an increase in temperature and a change in the refractive index of the material with temperature. This change is negative for gases but may be either positive or negative for condensed matter depending on the internal structure of the material [1]. It is a non-local optical phenomenon as the refractive index change at some point depends on the laser intensity nearby. The response time is of the order of nanoseconds and is very slow as the time taken to change the temperature of the material can be long. Mathematically, this change in refractive index with temperature can be expressed by the following relation:

$$\tilde{n} = n_0 + \left(\frac{\mathrm{d}n}{\mathrm{d}T}\right)\tilde{T}_1, \tag{49}$$

where $(\mathrm{d}n/\mathrm{d}T)$ describes the temperature dependence of refractive index while $\tilde{T}_1$ accounts for the change in temperature due to incident laser field and obeys the heat transport equation

$$(\rho_0 C)\,\frac{\partial \tilde{T}_1}{\partial t} - \kappa \bigtriangledown^2 \tilde{T}_1 = \alpha \tilde{I}(r), \tag{50}$$

where $\rho_0 C$ denotes the heat capacity per unit volume, κ denotes the thermal conductivity and α the linear absorption coefficient of the material.

There are a number of effects that can occur due to thermal contributions to the nonlinearity such as the formation of thermally induced optical grating, pattern formation etc., which have been discussed in [20-22].

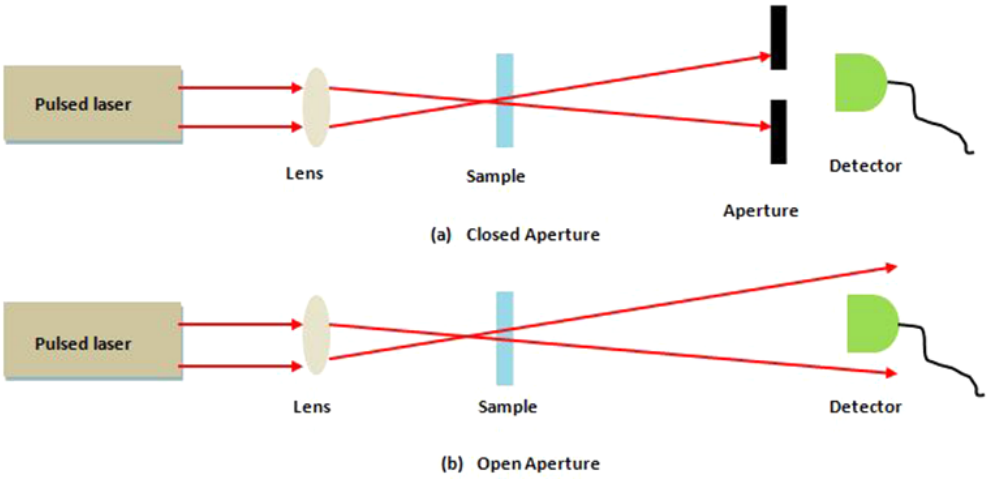

Fig. 15. – (a) Closed aperture scan schematic to measure real part of $\chi^{(3)}$. (b) Open aperture scan schematic to measure imaginary part of $\chi^{(3)}$.

7. – Measurement of optical nonlinearity: Z-scan

Z-scan, first reported in [23], is a single beam technique to measure both real and imaginary components of the nonlinear refractive index coefficient. To measure the real (refraction) coefficient, a tightly focussed Gaussian beam is made incident on the sample and the transmission through the nonlinear medium (assumed to be thinner than the diffraction length of the beam) is measured at the far-field through an aperture. The setup is shown in fig. 15.

To examine the effect of translation of the sample along the beam path, we consider a material with a negative value of n_2. We are ignoring the losses for the moment. When the sample is far away from the focus, due to low intensity of the optical field on the sample, there is no effect on the transmitted beam as the nonlinear contribution to the refractive index $n_2 I$ is very low. As the sample is moved from a negative z towards the focus, a negative lensing effect on the beam takes place prior to focus and the beam divergence at the aperture is reduced leading to increased transmission through the aperture. When the sample is moved beyond the focal plane towards positive z, the negative lensing effect causes defocussing at the aperture causing a decrease in transmission. This suggests that there is a null at the focus. The transmittance as a function of sample position for CS_2 is shown in fig. 16a. The peak-valley positions are reversed if the sample has a positive value of n_2 which is the case for CS_2.

When there are absorptive nonlinearities present, the transmittance curve shows asymmetrical peak and valley distribution. The presence of multi-photon absorption results in a larger valley while saturable absorption results in a larger peak. It is to be noted that the nonlinear refraction effect is probed by the aperture. When the aperture is removed from the far-field, the transmittance depends on absorption nonlinearities and there is no effect of nonlinear refraction. The transmittance obtained for an open

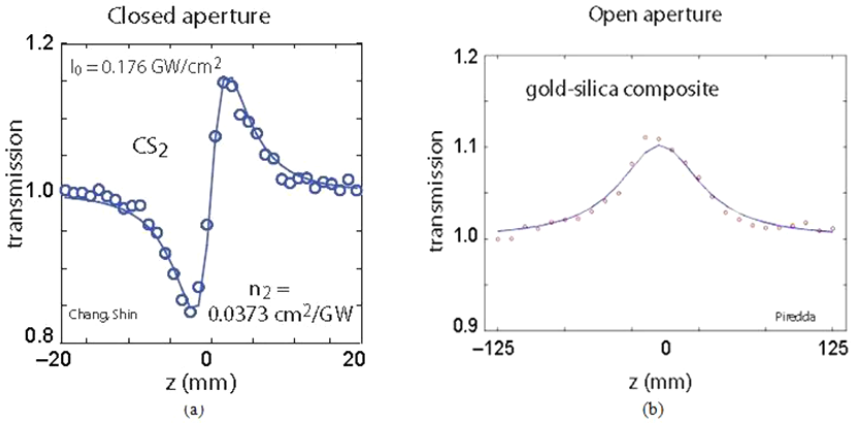

Fig. 16. – (a) Closed aperture scan result for CS_2 from Bahae *et al.* [23]. (b) Open aperture scan result for gold-silica composite [24].

aperture case is symmetrical with respect to the focus where the maxima (for saturable absorption) or the minima (for multi-photon absorption) occurs. Hence, the Z-scan measurement can not only be used to calculate the sign of nonlinear refraction, but the absorption mechanism within the sample as well. Compared to the other methods of measuring nonlinearity such as nonlinear interferometry [25, 26], degenerate four wave mixing [27], nearly degenerate three wave mixing [28], ellipse rotation [29] and beam distortion [30], Z-scan is a much simpler and sensitive process.

8. – Self-action effects

Self-action effects are effects in which a light beam modifies its own propagation by means of the nonlinear response of the medium. Common self-action effisre discussed briefly below.

8˙1. *Self-focussing*. – When an intense beam of light modifies the optical properties of the medium such that it is caused to come to a focus within the medium, the phenomenon is called self-focussing of light, or catastrophic collapse [1,31]. For a positive value of n_2, a beam with a varying transverse intensity profile induces refractive index variation with a maximum index at the centre of the beam that is larger than that at the periphery, creating a positive lens such that the beam comes to focus within the material. This situation results when the self-focussing effect is not compensated by diffraction or other nonlinearities (like quintic nonlinearity due to $\chi^{(5)}$). Also, the beam power P must be greater than the critical power for self-trapping, called $P_{\rm cr}$, so that the self-focussing effect is larger than diffraction and other defocussing effects.

Chiao *et al.* [32] give the following expression for $P_{\rm cr}$ assuming a circular beam of uniform intensity and radius w_0:

$$P_{\rm cr} = \frac{\pi(0.61)^2 {\lambda_0}^2}{8 n_0 n_2}\,, \tag{51}$$

where λ_0 is the vacuum wavelength of the applied optical field. The value of $P_{\rm cr}$ depends not only on the input beam profile, but is also different for bulk media and waveguides [33]. The distance at which the intensity becomes anomalously large is called the self-focussing length, $z_{\rm sf}$ or collapse length, $L_{\rm col}$ [31]. The expression for the self-focussing length $z_{\rm sf}$ given by Kelley is [31]

$$z_{\rm sf} = \frac{2n_0{w_0}^2}{\lambda_0}\frac{1}{\sqrt{P/P_{\rm cr}-1}}\,. \tag{52}$$

Note that $z_{\rm sf}$ scales with power as approximately $1/P^{1/2}$. For sufficiently high powers though, this collapse distance scales with $1/P$ as was demonstrated for cw beams propagating in CS_2 [34, 35].

In the previous cases, it was assumed that the input beams have no noise. But when noise is present, there is a second collapse threshold much greater than $P_{\rm cr}$, called $P_{\rm MF}$, where the input beam breaks up into multiple filaments for powers higher than $P_{\rm MF}$ as discussed by Fibich *et al.* in [36].

8˙2. *Optical solitons.* – An optical soliton is any optical field that does not change its shape (spatially or temporally) during propagation due to exact cancellation of nonlinear and linear focussing and defocussing effects within the medium. We can have two kinds of solitons depending on which profile, spatial or temporal, is preserved during propagation. A spatial soliton is formed due to exact cancellation of self-focussing and diffraction, while a temporal soliton is formed when there is cancellation of self-phase modulation and dispersion within the medium. We may also have a spatio-temporal soliton when all these effects balance simultaneously. We describe the spatial and temporal solitons in the following sections.

8˙2.1. Self-trapping and spatial solitons. When there is an exact balance between self-focussing and diffraction, the beam of light propagates with a constant diameter and the phenomenon is called self-trapping of light [32]. The power carried by the beam is exactly equal to the $P_{\rm cr}$, the critical power for self-trapping. Under these conditions, the beam forms its own waveguide and propagates without spreading. The nonlinear pulse propagation for this case is given by [1]

$$\bigtriangledown_T{}^2 A + 2ik\frac{\partial A}{\partial z} = -\frac{2k^2 n_2}{n_0}|A|^2 A, \tag{53}$$

which is also called the nonlinear Schrödinger equation (NLSE). The first term on the left accounts for diffraction while the term on the right accounts for self-focussing. When $A(x, y, z)$ varies along only one transverse dimension, say x, (or the case of a slab-shaped beam) the solution is called a spatial soliton and is given by

$$A(x, z) = A_0\,\mathrm{sech}(x/x_0)e^{i\gamma z}, \tag{54}$$

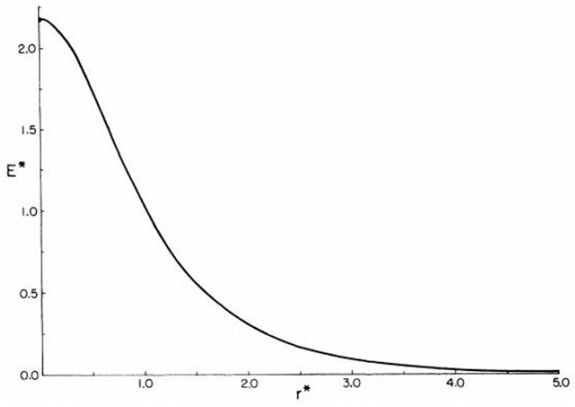

Fig. 17. – Radial profile of the self-focussed beam, also called the Townes profile [32].

where x_0 is the width of the field distribution of the soliton. For a cylindrical beam, where the transverse field variation has both x and y components, there is no analytic solution to the NLSE. The NLSE in cylindrical coordinates is written as

$$\frac{\mathrm{d}^2 A(r)}{\mathrm{d}r^2} + \frac{1}{r}\frac{\mathrm{d}A(r)}{\mathrm{d}r} - A(r) + A^3(r) = 0 \tag{55}$$

and the numerical solution, shown in fig. 17, is called the Townes profile [32].

In the absence of any saturation effects or plasma defocussing, this solution is not stable [37] and is susceptible to perturbations which might cause the beam to either diffract or self-focus [38]. However, when a beam self-focusses, the on-axis component evolves into the circularly symmetric Townes profile irrespective of the initial beam profile as discussed in [39] and [40] and the collapsed on axis portion carries exactly P_{cr} power. But for super-Gaussian beams, the beam self-focusses into a ring profile as reported in [41].

Spatial solitons can also be viewed as stationary wave packets that are localized in space. As such, they have the unique property that their energy and momentum is conserved even when they interact with each other leading to a number of interesting effects like soliton fusion, fission and annihilation [37]. The first spatial soliton was observed in a sodium vapor cell by Ashkin and Bjorkholm in 1974 [42]. Later on, spatial solitons were also observed in CS_2 in 1985 [43], in AlGaAs waveguides [44], and in nematic liquid crystals [45].

8˙2.2. Temporal solitons. When short optical pulses propagate within a non-dispersive, nonlinear medium, it experiences a nonlinear phase shift due to the medium's Kerr response [1]. If we assume that response of the medium is instantaneous, then the nonlinear phase shift experienced by an optical pulse of instantaneous pulse intensity $I(t)$ travelling through a medium of length L and central frequency ω_0 is

$$\phi_{\mathrm{NL}}(t) = -n_2 I(t)\omega_0 L/c. \tag{56}$$

This is known as self-phase modulation as a propagating optical pulse modifies its own phase due to the medium's nonlinearity as it propagates. This leads to spectral broadening. But in most instances, we also need to take into account the dispersion within a medium. For a pulse

$$\tilde{E}(t) = \tilde{A}(z,t)e^{i(k_0 z - \omega_0 t)} + \text{c.c.}, \tag{57}$$

the pulse propagation equation for a dispersive and nonlinear medium is given by [1]

$$\frac{\partial \tilde{A}_s}{\partial z} + \frac{1}{2} i k_2 \frac{\partial^2 \tilde{A}_s}{\partial \tau^2} = i\gamma \left| \tilde{A}_s \right|^2 \tilde{A}_s, \tag{58}$$

where

$$\tilde{A}_s(z,\tau) = \tilde{A}(z,t), \quad \tau = t - \frac{z}{v_g}, \tag{59}$$

with v_g being the group velocity. The second term on the left hand side of eq. (58) takes account of group velocity dispersion while the term on the right hand side takes account of self-phase modulation. Under proper circumstances, there can be an exact cancellation of the pulse spreading due to the two effects and the pulse shape is preserved as it propagates. These pulses are called temporal optical solitons. The fundamental solution for eq. (58) is given by

$$\tilde{A}_s(z,\tau) = A_s^0 \operatorname{sech}(\tau/\tau_0) e^{i\kappa z}. \tag{60}$$

Higher-order solutions to (58) have been discussed in [46] and [47]. Existence of temporal solitons in optical fibre was proposed in 1973 by Hasegawa and Tappert in [48]. Since then, many demonstrations of temporal solitons propagating over long distances have been demonstrated in [49, 50].

8˙3. *Small-scale filamentation.* – Small-scale filamentation, also known as beam breakup, is the breakup of an intense laser beam (with powers much higher than the P_{cr}) into multiple filaments, due to amplification of modulational instabilities and noise present in the optical wavefront by four-wave mixing [52]. The transverse intensity produced as a result may have a random distribution and reduced spatial coherence or may have highly regular pattern as shown in fig. 18 [51].

Each of the filaments produced are almost ideal solitons, have the cylindrically symmetric Townes profile and carry the power P_{cr} [53]. Figure 19 illustrates the amplification process of wavefront perturbations.

The field within the medium is composed of a strong on-axis component and weak, side-modes with non-collinear but symmetric k-vectors. The variation of gain coefficient of these side-modes with the magnitude of their wave vectors is shown in fig. 20. The peak value of the gain coefficient occurs when the four-wave mixing process is phase-matched.

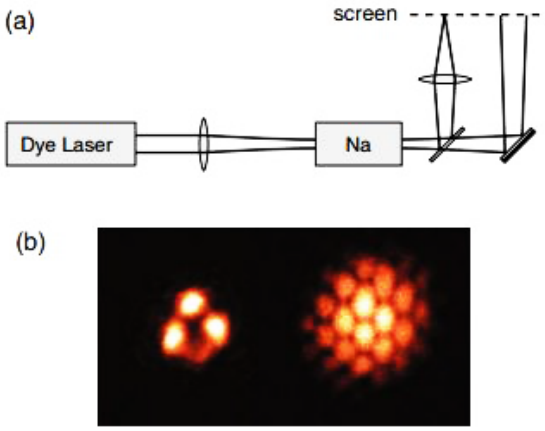

Fig. 18. – (a) Schematic of the experimental setup used in [51]. (b) Honeycomb pattern obtained in far-field.

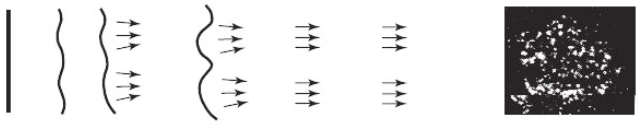

Fig. 19. – Amplification of wavefront perturbations to give multiple filaments.

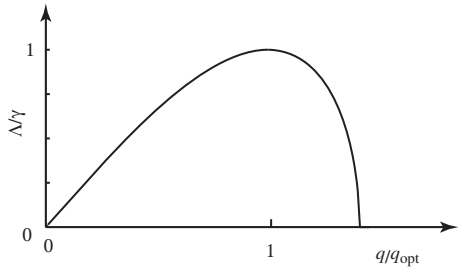

Fig. 20. – Gain coefficient of side-modes *vs.* wave vectors.

Beam breakup into multiple filaments have been reported by many groups in [54-60]. A possible application reported in [61] suggests that loss of spatial coherence can be used as a power limiter by reducing intensity at the focus (see fig. 21).

9. – Local-field effects

The treatment described above for calculating susceptibilities was based on macroscopic Maxwell equations which considers the spatial average of microscopic electric fields. But the actual atomic transitions within the material are dependent on the local field

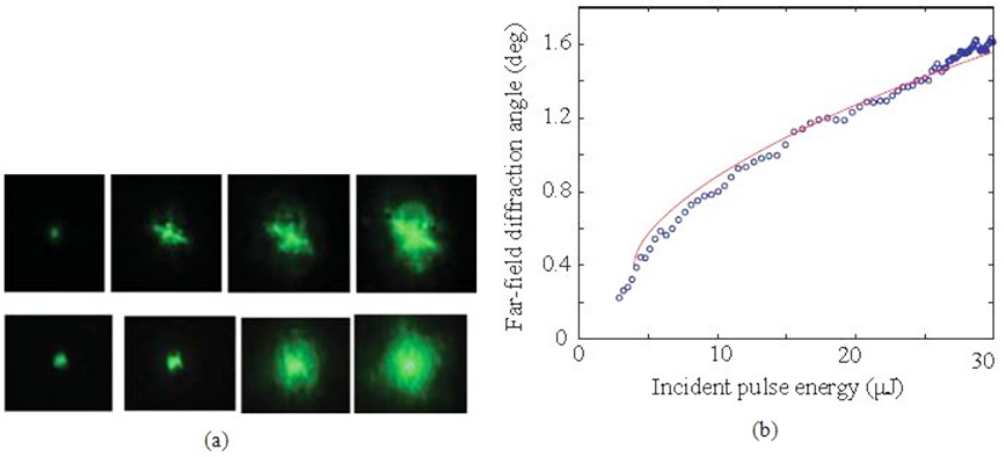

Fig. 21. – (a) Small-scale filamentation in CS_2. Top: near-field intensity distributions; bottom: far-field intensity distributions with increasing pulse energy from left to right. (b) Far-field diffraction angle *vs.* incident pulse energy showing a square-root variation of the angle.

which acts on the transition dipole moments associated with the material. For condensed matter, with atomic densities of the order of 10^{15} atoms/cm^3, the difference between the local field and the macroscopic field becomes significant and local field needs to be considered [62]. There are different models for performing local-field corrections depending on the optical medium under consideration. For a homogeneous medium, for example, we multiply the local-field correction factor L to the macroscopic field to calculate the local field. Different models applied to calculate L are: 1) the Lorentz local-field model, 2) the Onsager model, and 3) the real-cavity model. The Lorentz model and the Onsager model are applicable for homogeneous media, with Lorentz model used specifically for solids while Onsager model is used for polar liquids. The real-cavity model is used to describe composite materials [62]. The Lorentz model is the most commonly used model and is described in the following subsection.

9˙1. *Lorentz local field.* – The Lorentz-Lorenz law gives the following expression for the linear susceptibility [1]:

$$\chi^{(1)} = \frac{N\alpha}{1 - \frac{4\pi}{3}N\alpha} \quad \text{or} \quad \frac{\epsilon^{(1)} - 1}{\epsilon^{(2)} + 2} = \frac{4\pi}{3}N\alpha, \tag{61}$$

where N is the number density of dipoles within the medium (assumed to be a rectangular lattice) and α is the polarizability for a single dipole. The local field is expressed as the sum of local-field contributions for dipoles within the assumed cavity (with radius greater than dipole separation but less than optical wavelength), and the average macroscopic polarization for dipoles outside the cavity. Hence, the local field $\tilde{E}_{\text{loc}}$ is given (in Gaussian

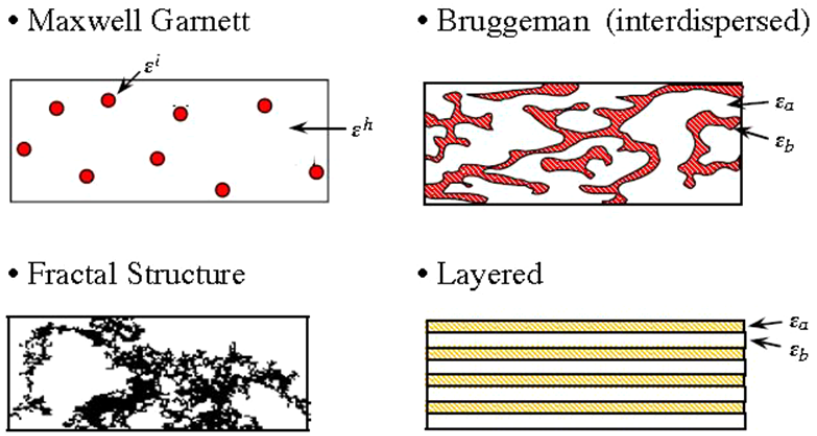

Fig. 22. – Examples of nanocomposite geometries that have been used to construct materials with enhanced nonlinear optical response [62].

units) by

$$\tilde{E}_{\rm loc} = \tilde{E} + \frac{4\pi}{3}\tilde{P}. \tag{62}$$

Since $\tilde{P} = \chi^{(1)}\tilde{E}$, the expression for local field is given by

$$\tilde{E}_{\rm loc} = \frac{\epsilon^{(1)} + 2}{3}\tilde{E}. \tag{63}$$

9˙2. *Nanocomposite materials for nonlinear optics.* – Local-field effects can substantially boost the nonlinear response. For example, it was shown in [4] that the expression for the third order susceptibility with local-field effects taken into account is

$$\chi^{(3)}(\omega_k = \omega_l + \omega_m + \omega_n, \omega_l, \omega_m, \omega_n) = N\gamma^{(3)}(\omega_k)L(\omega_k)L(\omega_l)L(\omega_m)L(\omega_n), \tag{64}$$

where $\gamma^{(3)}$ is the hyperpolarizability leading to the generation of the sum-frequency ω_k and the local-field correction factor is given by $L(\omega_i) = [\epsilon^{(1)}(\omega_1) + 2]/3$.

Composite materials are made of two or more constituents with different susceptibilities, and they can alter the local field substantially depending on the choice of materials and the configuration. Some examples of composite material structures are shown in fig. 22. We can tailor these composites to exhibit the desired optical properties. In fact, the composite material can possess an enhanced nonlinearity that can even exceed those of individual materials. Especially important are nanocomposite materials; these are nanoscale mixtures of different materials in which the individual particles are much smaller than the optical wavelength, but nonetheless are large enough so that they can be characterized by their own dielectric constants. Optical properties such as n_2 and $\chi^{(3)}$

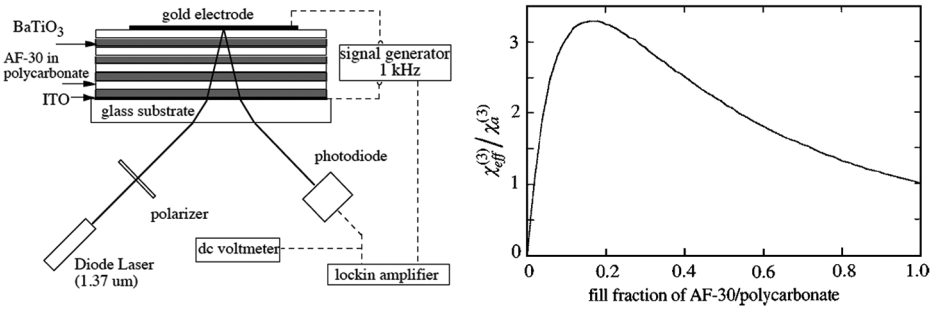

Fig. 23. – (a) Layered geometry and experimental setup used in [63]. (b) Predicted susceptibility enhancement curve.

of such materials are characterized by their effective or volume-averaged values. Some of these geometries are described in the following subsections.

9˙2.1. Layered composite materials. An example of a material with a layered geometry is shown in fig. 23a. It is composed of alternating layers of materials, say a and b, that have different optical properties and different thicknesses, which are assumed to be much smaller than the optical wavelength. The structural properties of each constituent are assumed to be essentially the same as for a bulk sample of such a material. The optical properties of the composite structure are dependent on the volume average of each constituent. For example, to enhance the contribution of material a to the nonlinear optical response of the composite, material b, must have a larger refractive index than material a. The enhancement of the $\chi^{(3)}$ response occurs as a result of the non-uniform distribution of the incident electric field between constituents a and b [64]. It was shown theoretically [65] that to have such an enhancement, the more nonlinear material, for instance material a, must have the smaller linear refractive index.

For p-polarized light incident on the layered composite, the effective permittivity ϵ_{eff} is given in terms of the volume fractions f_a and f_b and the permittivities of individual materials by [65]

$$\frac{1}{\epsilon_{\text{eff}}} = \frac{f_a}{\epsilon_a} + \frac{f_b}{\epsilon_b}. \tag{65}$$

Moreover, for the limiting case in which component b has a vanishingly small nonlinear response, the effective nonlinear response of the material becomes [65]

$$\chi^{(3)}_{\text{eff}} = \left|\frac{\epsilon_{\text{eff}}}{\epsilon_a}\right|^2 \left(\frac{\epsilon_{\text{eff}}}{\epsilon_a}\right)^2 f_a {\chi_a}^{(3)}. \tag{66}$$

For s-polarized light, the effective permittivities are

$$\epsilon_{\text{eff}} = f_a\epsilon_a + f_b\epsilon_b \quad \text{and} \quad \chi^{(3)}_{\text{eff}} = f_a\chi^{(3)}_a. \tag{67}$$

In [64], a layered geometry with alternating layers of titanium dioxide (material b) and the nonlinear optical polymer PBZT (material a) was investigated and a maximum enhancement of 35% of the third-order susceptibility was obtained which was experimentally measured in terms of the acquired nonlinear phase-shift by a propagating laser beam. In [63], the third-order susceptibility representing the electro-optic response of a layered composite material made of alternating layers of barium titanate and doped polycarbonate was investigated for different volume fill fractions. The predicted enhancement curve *vs.* fill fraction of the polycarbonate is shown in fig. 23b. One sees that an enhancement of the electro-optic response by a factor as large as 3.2 can be obtained.

9˙2.2. Metal-dielectric photonic crystals. Metals possess a very large and fast intrinsic nonlinear response. For example, the $\chi^{(3)}$ value of noble metals is 10^6 times higher than fused silica and has a sub-picosecond response [66]. However, it has proven difficult to access this nonlinearity due to high attentuation associated with metals. Due to this high attenuation, metals structures with a thickness larger than tens of nm are non-transmitting. Attempts to circumvent this high loss using local-field effects have been made by using colloidal metal nanoparticles [67], granular metal films [68], glasses doped with nanoparticles [66] and metal-dielectric composites in Maxwell-Garnett [69] and Bruggeman geometries [70, 71].

It has been shown [72] that a metal-dielctric photonic crystal (MDPC) can be highly transmissive within a certain controllable spectral range for metal thicknesses even larger than the skin depth. Such a MDPC was proposed [73] and demonstrated [24] as a nonlinear photonic material. It was argued [72, 73], that, since the large attenuation of light in metals is more due to re-radiation than absorption, a method akin to Bragg reflection can be employed to redirect the light in the forward direction. Figures 24a and 24b compare the electric field distribution within a bulk Cu sample of thickness 40 nm and a MDPC with alternating layers of gold and silica of thicknesses 16 nm and 98 nm respectively, having resonance at 650 nm. Due to the resonance nature of the structure, the nonlinearity was measured in terms of the fractional change in nonlinear transmission and reflection and the comparison with bulk metal values is shown in figs. 24c and d.

9˙3. *Counterintuitive consequence of local-field effects.* – In ref. [74], it was demonstrated that local-field effects can be used for sign reversal of the nonlinear absorption process. A colloid of metal nanoparticles in a glassy matrix showed saturable absorption, due to local-field correction even though the metal and glass themselves showed induced absorption. For a composite material consisting of a host material h (with permittivity ϵ_h) and inclusions i (with permittivity ϵ_i) the effective permittivity of the medium as a whole can be written in terms of the fill-fraction f of the inclusions

$$\epsilon = \epsilon_h \frac{1 + 2\eta f}{1 - \eta f}\,, \tag{68}$$

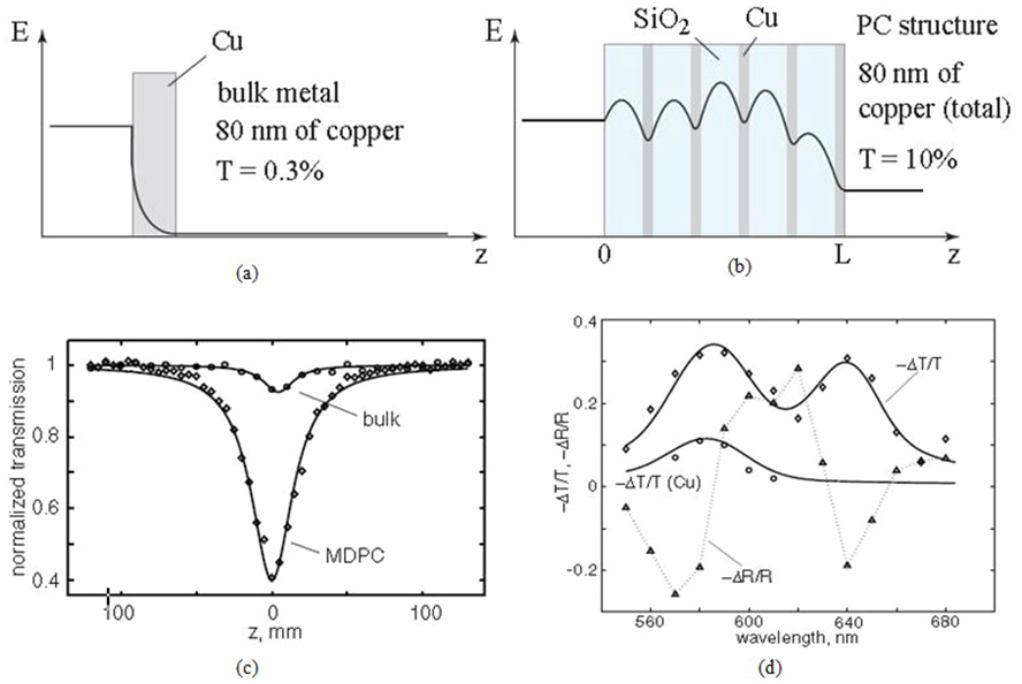

Fig. 24. – (a) Electric field distribution within bulk copper, (b) electric field distribution within the MDPC, (c) normalized transmission measured for bulk copper and the MDPC using the Z-scan method, and (d) measured fractional nonlinear change in reflection and transmission for bulk copper and for the MDPC.

where

$$\eta = \frac{\epsilon_i - \epsilon_h}{\epsilon_i + 2\epsilon_h}\,. \tag{69}$$

The third-order susceptibility can be written as

$$\chi^{(3)} = f{q_i}^2|q_i|^2{\chi_i}^{(3)} + {q_h}^2|q_h|^2\left[(1-f) + xf\right]{\chi_h}^{(3)}, \tag{70}$$

where

$$x = \frac{8}{5}\eta^2|\eta|^2 + \frac{6}{5}\eta|\eta|^2 + \frac{8}{5}\eta^3 + \frac{18}{5}(\eta^2 + |\eta|^2) \tag{71}$$

q_i and q_h are the local-field factors for the host and inclusions, respectively, and are given by

$$q_i = \frac{\epsilon + 2\epsilon_h}{\epsilon_i + 2\epsilon_h}\,, \tag{72}$$

$$q_h = \frac{\epsilon + 2\epsilon_h}{3\epsilon_h}\,. \tag{73}$$

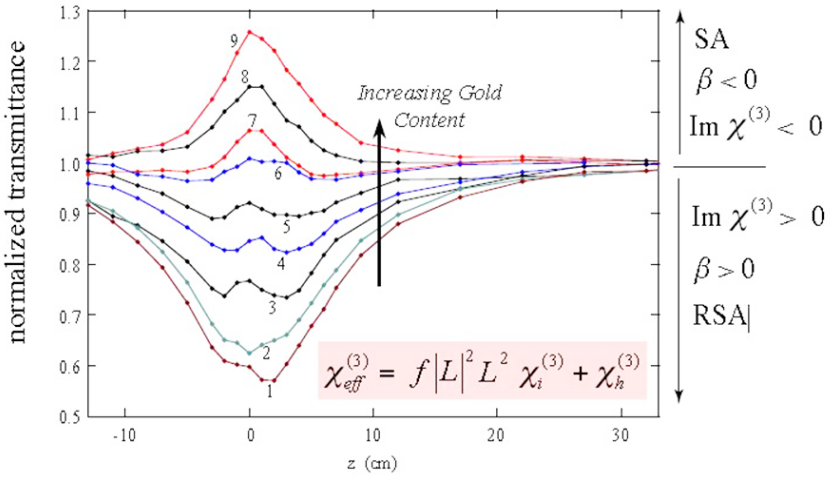

Fig. 25. – Normalized transmission curves obtained from Z-scan measurements showing reversal of the sign of $\mathrm{Im}[\chi^{(3)}]$.

For small fill-fractions, $\epsilon \simeq \epsilon_h$ and $q_h \simeq 1$. So the effective $\chi^{(3)}$ becomes

$$\chi^{(3)} = f {q_i}^2 |q_i|^2 \chi_i^{(3)} + \chi_h^{(3)}. \tag{74}$$

Even though the sign of both contributions to $\chi^{(3)}$ is the same, we can have cancellation of the two at surface-plasmon resonance due to the condition

$$\mathrm{Re}[\epsilon_i(\omega_s)] = -2\,\mathrm{Re}[\epsilon_h], \tag{75}$$

where ω_s is the surface plasmon resonance frequency. The local-field factor for the inclusions, q_i, then becomes purely imaginary since $q_i \approx 3\,\mathrm{Re}[\epsilon_h]/i\,\mathrm{Im}[\epsilon]$. Thus, at the surface plasmon resonance, ${q_i}^2 < 0$. If $\chi_i^{(3)}$ and $\chi_h^{(3)}$ have the same sign, for a particular fill-fraction f we have sign reversal of $\chi^{(3)}$.

Physically, we have a phase-difference between the field within inclusion and the externally applied field which is essentially given by the phase of q_i. This phase-difference becomes $\pi/2$ at surface plasmon resonance making q_i imaginary. This phase-shift occurs due to coupling of the p-polarized component of incident light with arbitrary polarization into surface-plasmons at resonance. If $\chi_i^{(3)}$ and $\chi_h^{(3)}$ have the same sign, the sign-reversal occurs at two fill-fractions f, as can be seen from eq. (74). But only the lower fill-fraction is feasible as higher values of f lead to higher nonlinear absorption. In [74], a colloid of gold in $1, 1', 3, 3, 3', 3'$-hexamethylindotricarbocyanine iodide (HITCI) (a reverse-saturable absorber), methanol and water showed this sign-reversal in $\mathrm{Im}[\chi^{(3)}]$ which can be seen in fig. 25 showing open-aperture Z-scan traces. Curves 1-5 have a valley indicating reverse-saturable absorption, whereas 6-9 have a peak, showing saturable absorption.

10. – Nonlinear plasmonics

Reasons for using plasmonic response in the context of nonlinear optics and photonics include the following:

1) Strong local-field enhancement: Surface plasmon polaritons (SPP) and localized surface plasmons (LSP) can provide very strong local-field enhancements [75].
2) Ultrafast response: Plasmonic excitations can respond on the scale of femtoseconds, making ultrafast signal processing possible [76].
3) Plasmon resonances are very sensitive to the dielectric constant of surrounding media [77]. This fact allows for the tailoring of the plasmonic response.
4) Sub-wavelength dimensions: At the nanoscale, plasmonic structures have very sub-wavelength dimensions and phase-matching is not important. Thus the nonlinear optical signal is emitted in all directions, irrespective of the propagation direction of the incident field and is incoherent [78].

Limiting factors to plasmonic responses are ohmic and radiative losses, which not only reduce the propagation length of SPP but also the local-field enhancement.

SHG using plasmonic structures has been achieved using different configurations. The very first example employed SHG from surface enhancement using roughened silver surfaces [79] where there was considerable enhancement of the SHG signal compared to a flat surface. Other methods employing surface enhancement have been reported in [80, 81]. Third-harmonic generation due to surface enhancement has also been reported in [82]. SHG from individual nano-particles such as gold nano-spheres [83], nano-cones [84], nano-apertures [85] and nano-cups [86] have also been reported. Structured plasmonic surfaces which are non-centrosymmetric like arrays of split ring resonators (SRR) [87], arrays of L-shaped nano-antennas [88] have also been reported to have enhanced SHG.

The intrinsic nonlinear response of SPPs has been explored [89] for gold films. These results showed a strong wavelength dependence of the nonlinear refraction as well as increase in the nonlinear absorption with larger pulse durations. This increase in nonlinear absorption was attributed to the "hot-electron" effect or "Fermi-smearing" mechanism, which is a kind of thermal effect with a sub-picosecond response.

11. – Slow and fast light

The group velocity of light is the velocity of propagation of the envelope of a light pulse. It can be represented mathematically as $v_g = c/n_g$ where we have introduced the group index [90]

$$n_g = n + \omega \frac{\mathrm{d}n}{\mathrm{d}\omega}\,, \tag{76}$$

where n is the refractive index and ω is the frequency of light. The phase velocity is the velocity with which points of constant phase of an optical field propagate within the medium and is equal to c/n. When light propagates in a medium for which the group velocity v_g is much smaller than the speed of light in vacuum, that is, for $v_g \ll c$, the phenomenon is

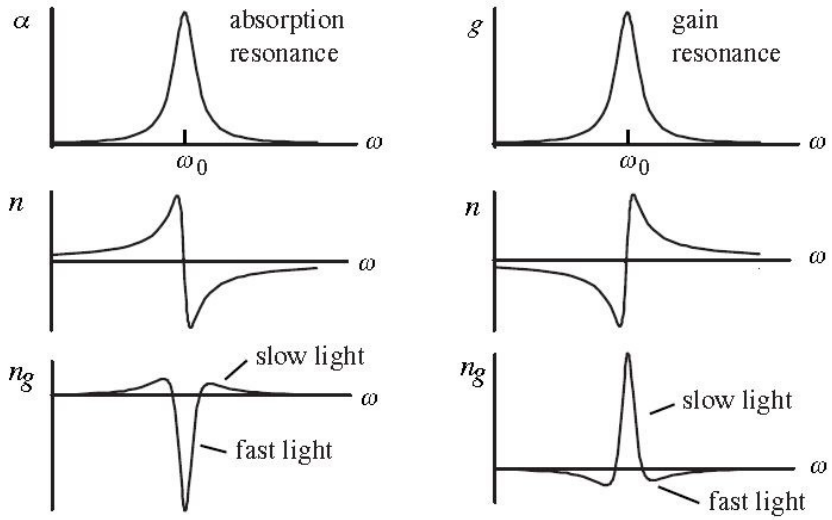

Fig. 26. – Dispersion curves for absorption and gain resonances.

called slow light. Fast light occurs when the group velocity becomes larger than c, which is also called superluminal propagation, or when v_g is negative, which is also known as backward propagation. From the expressions for the group index and group velocity, it is clear that a higher group index results in a lower group velocity, which is possible if the value of $\mathrm{d}n/\mathrm{d}\omega$ is large and positive, which is possible in the case of normal dispersion. For fast light, $\mathrm{d}n/\mathrm{d}\omega$ must be large and negative, which is possible for anomalous dispersion [91, 92]. Thus, resonant systems having an absorption (gain) resonance can be used to achieve slow (fast) light. To examine this argument more fully, let us consider the plots of the absorption, gain α and refractive index n *vs.* ω as shown in fig. 26. The motivation is distortion-free propagation of pulses through media with different group indices.

At the resonance, the absorption (gain) has a maxima and due to Kramers-Kronig relations, the refractive index makes a transition from maxima (minima) to minima (maxima). This steep transition results in a large value of $\mathrm{d}n/\mathrm{d}\omega$ and consequently in a lower or higher group velocity depending on the sign of $\mathrm{d}n/\mathrm{d}\omega$. For resonances in an atomic vapor, this group index can become as large as 10^4. But close to resonance the absorption also becomes large, and the slow (fast) is no longer easily measurable. The first experimental observation of slow light and fast light in resonant systems with negligible pulse distortion was by Carruthers and Bieber in 1969 [93]. But these results were limited by the presence of strong resonant absorption. To counteract the effect of large absorption, many schemes have been employed such as electromagnetically induced transparency (EIT) [94], coherent population oscillation (CPO) [95-98], stimulated Brillouin scattering (SBS) [97-99], stimulated Raman scattering (SRS) [100] and couple resonator pptical waveguides (CROWs) [101]. A very important experiment using Bose-Einstein

condensates achieved slow light with group velocity of 17 m/s using EIT [94]. EIT was first described theoretically by Harris *et al.* [102] and is a technique in which, under the influence of a large saturating optical field, the material is rendered transparent to resonant laser light. In the experiment of Hau *et al.* [94], the nanokelvin temperatures of the sample caused reduced Doppler broadening making the dispersion curve very steep leading to such a low group velocity. EIT was also used later by Budker *et al.* in a Rb vapor cell to achieve group velocities as low as 8 m/s [103]. Smilar technique was used later to achieve "stopped-light" [104].

Similarly, electromagnetically induced absorption has been used to achieve superluminal propagation, or fast light in [105] with group velocity of $-c/23\,000$. Since slow light has possible applications for tunable optical delays, optical memories, and data storage, a slow light source at room temperature is desirable. Some techniques to achieve slow light at room temperatures are described in the following subsections.

11˙1. *Slow light using SBS.* – Slow light using SBS in single-mode optical fibres at telecommunication wavelengths has been demonstrated [97, 99]. In this case, we have counterpropagating signal waves (ω) and pump waves (ω_p) within the fiber, and the maximum delay is produced when the signal frequency corresponds to Brillouin resonance frequency, *i.e.* $\omega = \omega_p - \Omega_B$, where Ω_B is the Brillouin frequency. Due to a lowered group velocity, one observes a delay in the pulse propagation time, which can be adjusted by varying the intensity I_p of the pump beam. The SBS process is a gain process in which the generated Stokes wave undergoes amplification by means of its coupling with the pump wave and an acoustic wave [1, 47]. Mathematically, the signal intensity variation with pump and signal is expressed as

$$\frac{\mathrm{d}I_s}{\mathrm{d}z} = -gI_sI_p \quad \text{where} \quad g = g_0\frac{(\Gamma_B)}{\Gamma_B + 2i(\omega - \omega_p)}\,. \tag{77}$$

Here g is the complex gain factor associated with the SBS process. The nonlinear refractive index n_2 thus depends on the imaginary part of g from which the propagation vector, k_s, and subsequently the group velocity can be calculated as $v_g = (\mathrm{d}k_s/\mathrm{d}\omega)^{-1}$. The transit time difference for a medium of length L can be subsequently calculated, as discussed in ref. [91]. Figure 27 shows the temporal evolution of Stokes pulses for a given gain value and different pulse lengths. There are several limiting processes that limit the observed delay, such as higher-order dispersion effects for very short pulse lengths, gain saturation for very high input Stokes pulse intensities, and spontaneous Brillouin scattering for very high gain values.

11˙2. *Slow light by coherent population oscillations.* – Coherent population oscillations are a quantum effect that lead to the creation of a spectral hole in the absorption profile of a probe beam passing through an appropriate medium. These population oscillations are a periodic modulation of the ground state populations at the beat frequency δ between the pump and probe waves. For $\delta \leq (1/T_1)$, with T_1 being the population relaxation time, these population oscillations have a significant magnitude. This method of introducing a

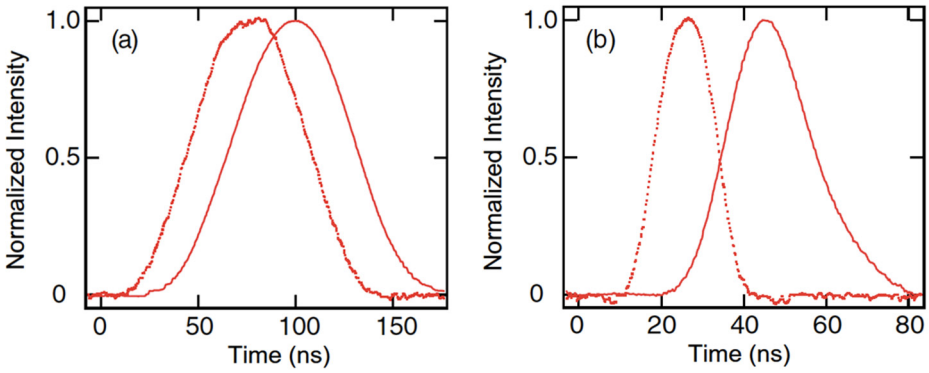

Fig. 27. – Temporal evolution of Stokes pulses for (a) 63 ns duration pulse, (b) 15 ns duration pulse.

spectral hole in a homogeneously broadened absorption spectrum was first predicted by Schwartz and Tan in [106] and was demonstrated by Hillman *et al.* for the case of a ruby crystal pumped by an Ar ion laser [107]. Slow light using this method of introducing a spectral hole was demonstrated in a ruby crystal where group velocities as low as 57.5 ± 0.5 m/s was observed in [96]. Here, a laser input at 514.5 nm from an Ar ion laser with pulse duration of the order of 1 ms was amplitude modulated to create frequency-shifted pump beams which were then focussed tightly within the crystal. A very narrow spectral hole of linewidth (HWHM) 35.8 Hz was observed which broadens with increased power. It is this narrow dip in the absorption profile that leads to very large values of

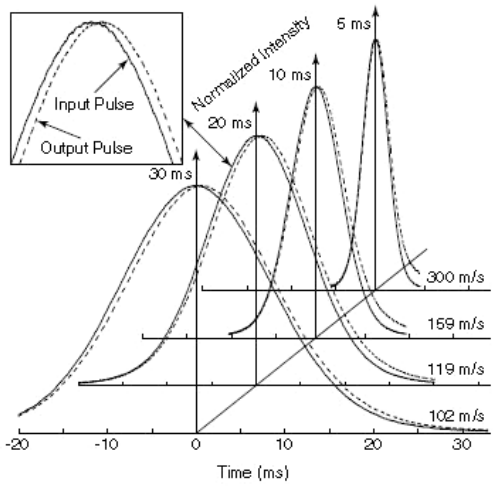

Fig. 28. – Normalized input and output pulse intensities for different pulse durations.

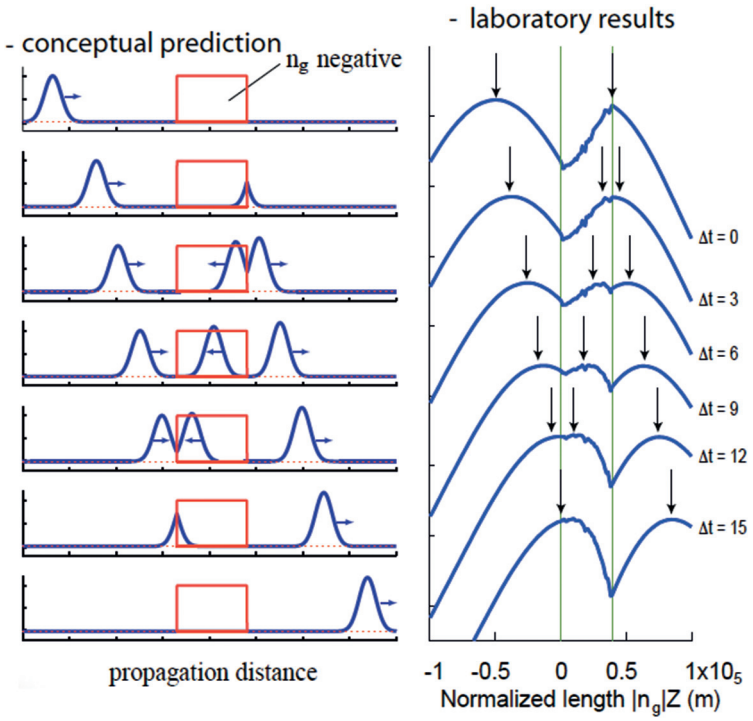

Fig. 29. – Left: Conceptual prediction of superluminal propagation. Right: Laboratory results of Bigelow *et al.* (2003) [95].

$dn/d\omega$ and hence very low group velocities. Figure 28 shows the different pulse delays with increased pulse durations.

Coherent population oscillations have also been used to achieve superluminal propagation in alexandrite due to formation on an anti-hole (increased absorption in a narrow spectral region) [95]. The superluminal response obtained in laboratory is shown in fig. 29.

11˙3. *Slow and fast light in Erbium-Doped Fibre Amplifiers (EDFAs).* – Slow and fast light has been successfully demonstrated [98] using the nonlinear optical response of EDFAs. The mechanism is that of coherent population oscillations (CPOs) involving the erbium ground-state population. Because of the widespread use of EDFAs in telecommunications, a slow-light source using EDFA has many potential important applications. Also, the use of fibre allows longer interaction lengths causing even larger delays. The width of the spectral hole is determined by the frequency of the population oscillations. Figure 30 shows the dependence of the fractional pulse advancement on both modulation frequency and on laser power.

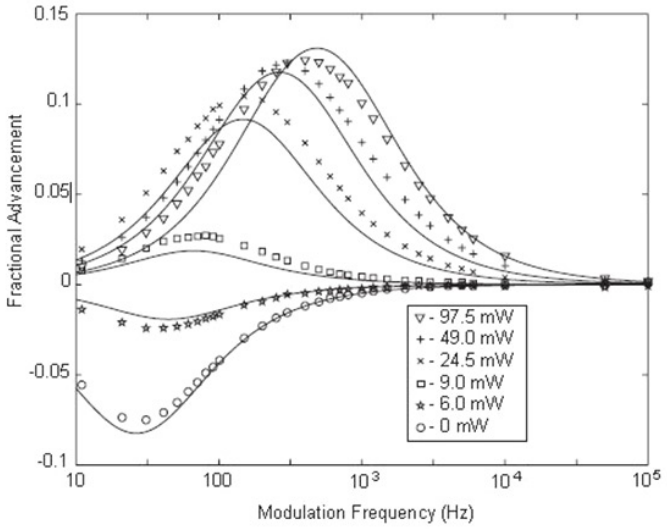

Fig. 30. – Dependence of fractional pulse delay after propagation through EDFA on the pump frequency and power.

12. – Spontaneous and stimulated light scattering

Until now, we have dealt with parametric processes which involve light-by-light scattering. We will now discuss inelastic scattering of light by various material media. Light scattering occurs due to fluctuations and inhomogeneities in optical properties of the medium. A completely homogeneous medium cannot scatter light into directions other than the exact forward direction, as a consequence of complete destructive interference that occurs in other directions [108]. Scattering into the forward direction is fully coherent and is the origin of the index of refraction [109].

Figure 31 illustrates this concept where we see that if the density of the material is uniform, the contribution due to molecules in volume dV_1 exactly cancels that due to molecules in dV_2 in all other directions except forward, while for a non-uniform material density, these contributions do no exactly cancel out. Light scattering can be classified

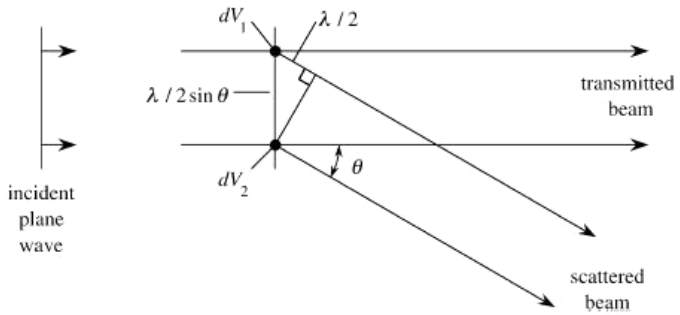

Fig. 31. – Light scattering in a material medium.

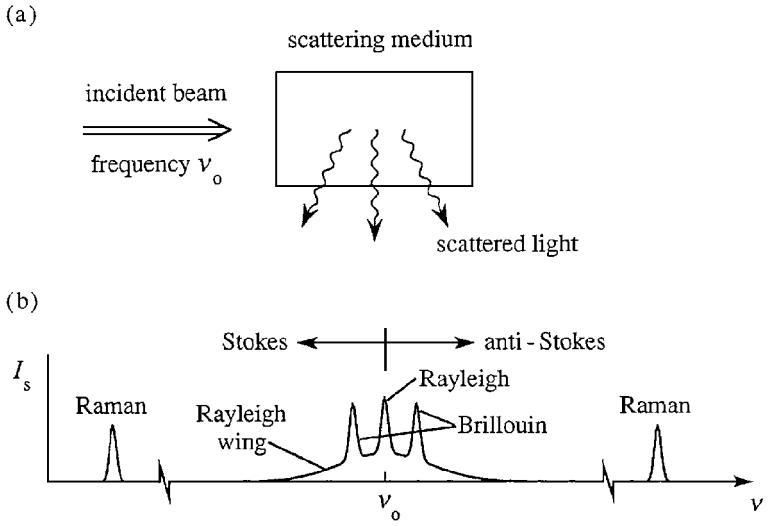

Fig. 32. – (a) A general light scattering experiment, (b) Spectrum of the scattered light showing source of various frequency components.

as stimulated or spontaneous depending on whether or not the fluctuations responsible for the scattering are induced by the incident laser field.

Let us next consider the most general case of a light scattering experiment as shown in fig. 32a. When we examine the spectrum of the scattered light, as shown in fig. 32b, we find contributions from different scattering mechanisms such as Rayleigh, Raman, Brillouin and the distant wing of the Rayleigh line. The frequency components of scattered light which are lower (higher) than that of the incident field are called Stokes (anti-Stokes) [1]. Raman scattering occurs due to interaction of light with the vibrational modes of molecules of the medium and is equivalent to scattering from optical phonons. Brillouin scattering occurs due to scattering of light from propagating density waves or sound waves and is equivalent to scattering from acoustic phonons. Rayleigh scattering on the other hand occurs due to static or non-propagating density fluctuations and is quasi-elastic in nature as it induces no frequency shift. Rayleigh-wing scattering occurs in anisotropic molecules due to fluctuations in molecular orientation and due to a very rapid reorientation of molecules, has a very broad spectrum. Table III states the typical linewidth, frequency-shifts, relaxation times and gain for the different light scattering processes.

12˙1. *Stimulated light scattering*. – Spontaneous light scattering is a weak process and the efficiency is quite low even for condensed matter. Stimulated processes on the other hand can be highly efficient. Also, the emission from spontaneous scattering is in the form of a dipole, while that for a stimulated light scattering is in the form of a narrow cone in the forward or the backward direction [1]. Conceptually, there are two separate configurations for studying stimulated light scattering [1]:

1) The generator configuration: In this case, only the pump beam is applied externally

TABLE III. – *Typical values of parameters for different light scattering processes.*

Process	Shift (cm^{-1})	Linewidth (cm^{-1})	Relaxation Time (s)	Gain (m/MW)
Raman	1000	5	10^{-12}	5×10^{-5}
Brillouin	0.1	5×10^{-3}	10^{-9}	10^{-4}
Rayleigh	0	5×10^{-4}	10^{-8}	10^{-6}
Rayleigh-wing	0	5	10^{-12}	10^{-5}

to the scattering medium, and the Stokes signal wave and phonon wave are created from noise within the medium. This process is shown in fig. 33a. For stimulated Brillouin scattering (SBS), the Stokes wave is amplified in all directions except in the exact forward direction, although it is usually observed only in the backward direction due to maximum spatial overlap with the pump in this case. Conversely, for stimulated Raman scattering (SRS), the Stokes signal is emitted in both the forward and backward directions.

2) The amplifier configuration: In this configuration, as shown in fig. 33b, both the pump and a weak Stokes seed signal are applied externally to the medium, and both the Stokes signal and the phonon waves are amplified. A strong coupling between the Stokes beam and pump occurs only when the frequency of the seed is close to the Stokes frequency of the generator case.

Hellwarth in [110] has explained the fundamental relation between spontaneous and stimulated light scattering in terms of the photon occupation numbers in different field modes. He argues that the probability per unit time P_S for a photon to be emitted into Stokes mode S is given by

$$P_S = Dm_L(m_S + 1), \tag{78}$$

where m_L is the mean number of photons per mode in the incident laser field, m_S is the number of photons in the Stokes mode and D is the proportionality constant that depends

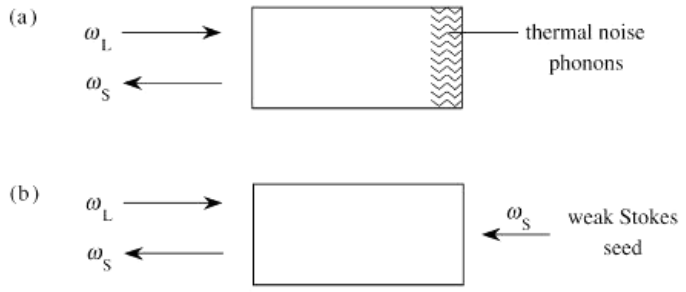

Fig. 33. – (a) Generator configuration for SBS; (b) amplifier configuration for SBS.

on the physical properties of the medium. From this assumption, one can deduce that the rate of change of the number of photons in a given Stokes mode for a wave traveling in the positive z direction with velocity c/n is given by

$$\frac{\mathrm{d}m_S}{\mathrm{d}z} = \frac{1}{c/n} D m_L (m_S + 1). \tag{79}$$

For the case of spontaneous emission, the occupation number in Stokes mode can be assumed to be much smaller than unity and the solution of eq. (79) becomes

$$m_S(z) = m_S(0) + \frac{1}{c/n} D m_L z. \tag{80}$$

Hence, the Stokes intensity increases linearly with the length of the Raman medium. For the case of stimulated scattering, the number of photons contained in the Stokes mode can be assumed to be much larger than unity, which leads to the prediction

$$m_S(z) = m_S(0) e^{Gz} \quad \text{where} \quad G = \frac{D m_L}{c/n}\,, \tag{81}$$

where G is the Raman gain coefficient. Thus, the Stokes intensity for a stimulated scattering case increases exponentially with z. The significance of this result is that Hellwarth was able to obtain an equation that relates the gain coefficient G of the stimulate process to the quantity D that quantifies the efficiency of the spontaneous process. For this reason, Hellwarth's result is sometimes said to show that for any spontaneous light scattering process there is a stimulated analog.

12˙1.1. Stimulated Brillouin scattering (SBS). Spontaneous Brillouin scattering was first predicted theoretically in 1918 by Mandelstam [111] and then later independently by Brillouin [112] in 1922. Gross [113] provided the first experimental evidence of Brillouin scattering in crystals and liquids. Figure 34 shows the scattering of an incident laser beam of frequency ω_L with a travelling pressure (or density wave) *i.e.* a sound wave of frequency Ω.

Due to the acoustic wavefronts travelling away from the incident laser wave, the scattered light is shifted downward in frequency leading to a Stokes wave with frequency $\omega_S = \omega_L - \Omega$. The interference of this pump wave and the Stokes wave leads to a wave of frequency $\omega_L - \omega_S$ which is of course equal to Ω and thus the acoustic wave is reinforced. This acoustic wave further beats with the incident laser field leading to Stokes wave and so on. This situation leads to a kind of positive feedback system which under proper circumstances leads to amplification of both the Stokes wave and the acoustic wave exponentially [1]. There are two different mechanisms for Stokes wave amplification due to the acoustic wave and the laser field:

1) Electrostriction: In the presence of a high optical intensity, materials have the tendency to become more compressed, leading to increased density. Here, the

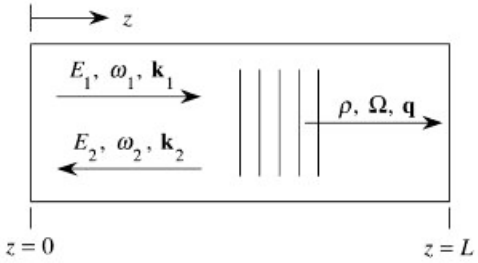

Fig. 34. – Scattering of an incident laser beam with sound wave.

interference between the Stokes wave and the laser field leads to fringes of high and low light intensity which show density variation due to electrostriction and hence lead to a propagating density wave or acoustic wave.

2) Optical Absorption: In regions of high optical intensity, heat generation can cause material expansion leading to decreased density on those regions. This process also leads to the generation of an acoustic wave.

Let us consider the case of an SBS generator as shown in fig. 33a. From the phonon dispersion relation $\Omega_B = |q_B|v$ and momentum conservation, we get the expression for Brillouin frequency as

$$\Omega_B = \frac{\frac{2v}{c/n}\omega_1}{1 + \frac{v}{c/n}}\,. \tag{82}$$

Since nv/c is very small for most cases, we can approximate the Brillouin frequency as

$$\Omega_B = \frac{2v}{c/n}\omega_1. \tag{83}$$

For the case of an SBS amplifier, the Stokes frequency ω_2 is determined by the laboratory settings and the acoustic wave frequency is given by $\Omega = \omega_1 - \omega_2$. In a sense the Stokes frequency ω_2 is arbitrary, but the acoustic wave is efficiently excited only when the Stokes seed frequency is chosen such that Ω lies within the Brillouin linewidth Γ_B. If we consider the coupled-amplitude equations for the SBS amplifier case, we see that there is no phase mismatch term, indicating that SBS is a pure gain process and is automatically phase-matched. Hence, we can write the coupled-intensity equations as

$$\frac{\mathrm{d}I_1}{\mathrm{d}z} = -gI_1I_2, \tag{84}$$

$$\frac{\mathrm{d}I_2}{\mathrm{d}z} = -gI_1I_2, \tag{85}$$

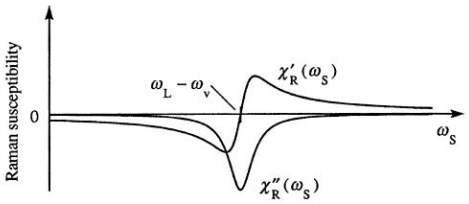

Fig. 35. – Real and imaginary parts of Raman susceptibility.

where g is the SBS gain factor given by

$$g = g_0 \frac{(\Gamma_B/2)^2}{(\Omega_B - \Omega)^2 + (\Gamma_B/2)^2}, \qquad g_0 = \frac{\gamma_e^2 \omega_2}{nvc^3 \rho_0 \Gamma_B}. \tag{86}$$

For a constant pump intensity, the output intensity for a medium of length L is given by

$$I_2(z) = I_2(L) e^{gI_1(L-z)}. \tag{87}$$

12˙1.2. Stimulated Raman scattering (SRS). C.V. Raman discovered the spontaneous Raman scattering in 1930 [114]. Stimulated Raman scattering occurs when the incident optical field within a medium interacts with the vibrational modes of molecules. Let us consider the simplest, classical explanation of SRS as discussed in [115], where each vibrational mode is described by a simple harmonic oscillator with time-varying inter-nuclear distance as $\tilde{q}(t)$, resonance frequency ω_v, damping constant γ and equilibrium inter-nuclear separation as q_0. The equation of motion can be written as

$$\frac{\mathrm{d}^2\tilde{q}}{\mathrm{d}t^2} + 2\gamma \frac{\mathrm{d}\tilde{q}}{\mathrm{d}t} + {\omega_v}^2 \tilde{q} = \frac{\tilde{F}(t)}{m} \tag{88}$$

with $\tilde{F}(t)$ being the restoring force and m the reduced nuclear mass. It is assumed that the optical polarizability depends on the inter-nuclear separation $\tilde{q}(t)$ according to

$$\tilde{\alpha}(t) = \alpha_0 + \left(\frac{\partial \alpha}{\partial q}\right)_0 \tilde{q}(t), \tag{89}$$

where α_0 is the equilibrium polarizability. Oscillations in the molecular coordinate $\tilde{q}(t)$ lead to periodic modulations in the polarizability with time which in turn leads to variation in the refractive index with time as

$$\tilde{n}(t) = \sqrt{\tilde{\epsilon}(t)} = [1 + N\tilde{\alpha}(t)]^{1/2}. \tag{90}$$

This modulation in refractive index with time forms frequency sidebands on the transmitted light with frequency $\pm\omega_v$. These frequency sidebands then beat with the incident laser field to generate a Stokes wave with frequency $\omega_S = \omega_L - \omega_v$ and modulate the

intensity at the same frequency. This modulated intensity in turn coherently excites the molecule to oscillate at ω_v. From the expression for the polarizability α in eq. (89), we can derive the expression for Raman susceptibility which is given by

$$\chi_R(\omega_S) = \frac{\epsilon_0(N/6m)(\partial\alpha/\partial q)_0{}^2}{\omega_v{}^2 - (\omega_L - \omega_S)^2 + 2i(\omega_L - \omega_S)\gamma}\,. \tag{91}$$

The real and imaginary parts of Raman susceptibility are shown in fig. 35. The valley of the imaginary part of susceptibility denotes the Raman resonance.

* * *

The research was supported by the Canadian Excellence Research Chair (CERC) program. SC also acknowledges support through Società Italiana di Fisica.

REFERENCES

[1] BOYD R. W., *Nonlinear Optics*, third edition (Academic Press, Boston, MA) 2008.
[2] HELLWARTH R., CHERLOW J. and YANG T., *Phys. Rev. B*, **11** (1975) 964.
[3] WRIGHT J. K., *Contemp. Phys.*, **6** (1964) 1.
[4] BLOEMBERGEN N., *Nonlinear Optics* (Benjamin, New York) 1964.
[5] FRANKEN P. A., HILL A. E., PETERS C. W. and WEINRICH G., *Phys. Rev. Lett.*, **7** (1961) 118.
[6] TERHUNE R. W., MAKER P. D. and SAVAGE C. M., *Phys. Rev. Lett.*, **14** (1965) 681.
[7] VAN TRAN N., SPALTER J., HANUS J., ERNEST J. and KEHL D., *Phys. Lett.*, **19** (1965) 4.
[8] DOLGALEVA K., LEPESHKIN N. and BOYD R. W., *Frequency doubling*, in *Encyclopedia of Nonlinear Science*, edited by ALWYN SCOTT (Routledge, New York) 2004.
[9] SHEN Y. R., *The Principles of Nonlinear Optics* (Wiley, New York) 1984.
[10] BURNHAM D. C. and WEINBERG D. L., *Phys. Rev. Lett.*, **25** (1970) 84.
[11] HARRIS S. E., OSHMAN M. K. and BYER R. L., *Phys. Rev. Lett.*, **18** (1967) 18.
[12] RUBIN M. H., KLYSHKO D. N., SHIH Y. H. and SERGIENKO A. V., *Phys. Rev. A*, **50** (1994) 5122.
[13] KWIAT P. G., MATTLE K., WEINFURTER H., ZEILINGER A., SERGIENKO A. V. and SHIH Y., *Phys. Rev. Lett.*, **75** (1995) 4337.
[14] MIDWINTER J. E. and WARNER J., *Br. J. Appl. Phys.*, **16** (1965) 1135.
[15] KLEINMAN D. A., ASHKIN A. and BOYD G. D., *Phys. Rev.*, **145** (1966) 338.
[16] KLEINMAN D. A., *Phys. Rev.*, **128** (1962) 1761.
[17] BOYD G. D. and KLEINMAN D. A., *J. Appl. Phys.*, **39** (1968) 3597.
[18] KLEINMAN D. A., *Phys. Rev.*, **128** (1962) 1761.
[19] ARMSTRONG J. A., BLOEMBERGEN N., DUCUING J. and PERSHAN P. S., *Phys. Rev.*, **127** (1962) 1918.
[20] BENTLEY S. J., BOYD R. W., BUTLER W. E. and MELISSINOS A. C., *Opt. Lett.*, **26** (2001) 14.
[21] BENTLEY S. J., BOYD R. W., BUTLER W. E. and MELISSINOS A. C., *Opt. Lett.*, **25** (2000) 16.
[22] MARTIN G. and HELLWARTH R. W., *Appl. Phys. Lett.*, **34** (1979) 371.
[23] SHEIK-BAHAE M., SAID A. A., WEI T. H., HAGAN D. J. and VAN STRYLAND E. W., *IEEE J. Quantum Electron.*, **26** (1990) 760.

[24] Lepeshkin N. N., Schweinsberg A., Piredda G., Bennink R. S. and Boyd R. W., *Phys. Rev. Lett.*, **93** (2004) 123902.
[25] Weber M. J., Milam D. and Smith W. L., *Opt. Eng.*, **17** (1978) 463.
[26] Moran M. J., She C. Y. and Carman R. L., *IEEE J. Quantum Electron.*, **11** (1975) 259.
[27] Friberg S. R. and Smith P. W., *IEEE J. Quantum Electron.*, **23** (1987) 2089.
[28] Adair R., Chase L. L. and Payne S. A., *J. Opt. Soc. Am. B*, **4** (1987) 875.
[29] Owyoung A., *IEEE J. Quantum Electron.*, **9** (1973) 1064.
[30] Williams W. E., Soileau M. J. and Van Stryland E. W., *Opt. Commun.*, **50** (1984) 256.
[31] Kelley P. L., *Phys. Rev. Lett.*, **15** (1965) 1005.
[32] Chiao R. Y., Garmire E. and Townes C. H., *Phys. Rev. Lett.*, **13** (1964) 15.
[33] Fibich G. and Gaeta A. L., *Opt. Lett.*, **25** (2000) 5.
[34] Campillo A. J., Shapiro S. L. and Surdyam B. R., *Appl. Phys. Lett.*, **24** (1974) 178.
[35] Surdyam B. R., *IEEE J. Quantum Electron.*, **10** (1974) 837.
[36] Fibich G., Eisenmann S., Ilan B., Erlich Y., Fraenkel M., Henis Z., Gaeta A. L. and Zigler A., *Opt. Express*, **13** (2005) 15.
[37] Stegman G. I. and Segev M., *Science*, **286** (1999) 1518.
[38] Moll K. D., Gaeta A. L. and Fibich G., *Phys. Rev. Lett.*, **90** (2003) 20.
[39] Fibich G. and Ilan B., *J. Opt. Soc. Am. B*, **17** (2000) 1749.
[40] Gross B. and Manassah J. T., *Phys. Lett. A*, **169** (1992) 371.
[41] Grow T. D., Ishaaya A. A., Vuong L. T. and Gaeta A. L., *Opt. Express*, **14** (2006) 12.
[42] Bjorkholm J. E. and Ashkin A., *Phys. Rev. Lett.*, **32** (1974) 4.
[43] Barthelemy A., Maneuf S. and Froehly C., *Opt. Commun.*, **55** (1985) 3.
[44] Aitchison J. S. *et al.*, *Electron. Lett.*, **28** (1992) 1879.
[45] Beeckman J., Neyts K., Hutsebaut X., Cambournac C. and Haelterman M., *Opt. Express*, **12** (2004) 1011.
[46] Zakharov V. E. and Shabat A. B., *JETP*, **34** (1972) 63.
[47] Agrawal G. P., *Nonlinear Fiber Optics* (Academic Press, Boston) 1989.
[48] Hasegawa A. and Tappert F., *Appl. Phys. Lett.*, **23** (1973) 142.
[49] Mollenauer L. F., Stolen R. H. and Gordon J. P., *Phys. Rev. Lett.*, **45** (1980) 1095.
[50] Mollenauer L. F. *et al.*, *IEEE J. Quantum Electron.*, **22** (1986) 157.
[51] Bennink R. S., Wong V., Marino A. M., Aronstein D. L., Boyd R. W., Stroud C. R. jr., Lukishova S. and Gauthier D. J., *Phys. Rev. Lett.*, **88** (2002) 113901.
[52] Bespalov V. I. and Talanov V. I., *JETP Lett.*, **3** (1966) 307.
[53] Kip D., Soljacic M., Segev M., Eugenieva E. and Christodoulides D. N., *Science*, **290** (2000) 495.
[54] Berg L., Skupin S., Lederer F., Mjean G., Yu J., Kasparian J., Salmon E., Wolf J. P., Rodriguez M., Wste L., Bourayou R. and Sauerbrey R., *Phys. Rev. Lett.*, **92** (2004) 225002.
[55] Fibich G., Eisenmann S., Ilan B. and Zigler A., *Opt. Lett.*, **29** (2004) 15.
[56] Dubietis A., Tamoauskas G., Fibich G. and Ilan B., *Opt. Lett.*, **29** (2004) 10.
[57] Mchain G., Couairon A., Franco M., Prade B. and Mysyrowicz A., *Phys. Rev. Lett.*, **93** (2004) 3.
[58] Vidal F. and Johnston T. W., *Phys. Rev. Lett.*, **77** (1996) 7.
[59] Schroeder H., Liu J. and Chin S. L., *Opt. Express*, **12** (2004) 20.
[60] Vuong L. T., Grow T. D., Ishaaya A. A., Gaeta A. L., 'T Hooft G. W., Eliel E. R. and Fibich G., *Phys. Rev. Lett.*, **96** (2006) 13.
[61] Schweinsberg A., Kuper J. and Boyd R. W., *Phys. Rev. A*, **84** (2011) 053837.

[62] DOLGALEVA K. and BOYD R. W., *Adv. Opt. Photon.*, **4** (2012) 1.
[63] NELSON R. L. and BOYD R. W., *Appl. Phys. Lett.*, **74** (1999) 2417.
[64] FISCHER G. L., BOYD R. W., GEHR R. J., JENEKHE S. A., OSAHENI J. A., SIPE J. E. and WELLER-BROPHY L. A., *Phys. Rev. Lett.*, **74** (1995) 1871.
[65] BOYD R. W. and SIPE J. E., *J. Opt. Soc. Am. B*, **11** (1994) 297.
[66] TOKIZAKI T., NAKAMURA A., KANEKO S., UCHIDA K., OMI S., TANJI H. and ASAHARA Y., *Appl. Phys. Lett.*, **65** (1994) 941.
[67] HACHE F., RICARD D., FLYTZANIS C. and KREIBIG U., *Appl. Phys. A*, **47** (1988) 4.
[68] SHALAEV V. M., *Nonlinear Optics of Random Media* (Springer-Verlag, Berlin) 2000.
[69] MAXWELL GARNETT J. C., *Philos. Trans. R. Soc. Lond. A*, **203** (1904) 359.
[70] BRUGGEMAN D. A. G., *Ann. Phys.*, **24** (1935) 637.
[71] GEHR R. J., FISCHER G. L. and BOYD R. W., *J. Opt. Soc. Am. B*, **14** (1997) 2310.
[72] BLOEMER M. J. and SCALORA M., *Appl. Phys. Lett.*, **72** (1998) 1676.
[73] BENNINK R. S., YOUNG-KWON YOON, BOYD R. W. and SIPE J. E., *Opt. Lett.*, **24** (1999) 1416.
[74] SMITH D. D., FISCHER G., BOYD R. W. and GREGORY D. A., *J. Opt. Soc. Am. B*, **14** (1997) 1625.
[75] KAURANEN M. and ZAYATS A. V., *Nat. Photon.*, **6** (2012) 737.
[76] STOCKMAN M. I., *Opt. Express*, **19** (2011) 22029.
[77] HOMOLA J., *Chem. Rev.*, **108** (2008) 462.
[78] ANCEAU C., BRASSELET S., ZYSS J. and GADENNE P., *Opt. Lett.*, **28** (2003) 713.
[79] CHEN C. K., DE CASTRO A. R. B. and SHEN Y. R., *Phys. Rev. Lett.*, **46** (1981) 145.
[80] SMOLYANINOV I. I., ZAYATS A. V. and DAVIS C. C., *Phys. Rev. B*, **56** (1997) 9290.
[81] WOKAUN A. *et al.*, *Phys. Rev. B*, **24** (1981) 849.
[82] KIM E. M. *et al.*, *Phys. Rev. Lett.*, **95** (2005) 227402.
[83] DADAP J. I., SHAN J., EISENTHAL K. B. and HEINZ T. F., *Phys. Rev. Lett.*, **83** (1999) 4045.
[84] BOUHELIER A., BEVERSLUIS M., HARTSCHUH A. and NOVOTNY L., *Phys. Rev. Lett.*, **90** (2003) 013903.
[85] NAHATA A., LINKE R. A., ISHI T. and OHASHI K., *Opt. Lett.*, **28** (2003) 423.
[86] HANKE T. *et al.*, *Nano Lett.*, **12** (2012) 992.
[87] LINDENNET S. *et al.*, *Phys. Rev. Lett.*, **109** (2012) 015502.
[88] TUOVINEN H. *et al.*, *J. Nonlinear Opt. Phys. Mater.*, **11** (2002) 421.
[89] DE LEON I., SHI Z., LIAPIS A. C. and BOYD R. W., *Opt. Lett.*, **39** (2014) 2274.
[90] BRILLOUIN L., *Wave Propagation and Group Velocity* (Academic Press, New York) 1960.
[91] BOYD R. W. and GAUTHIER D. J., *Slow and fast light*, in *Progress in Optics* (Elsevier) 2002.
[92] CHIAO R. Y. and MILONNI P. W., *Opt. Photon. News*, **13** (2002) 26.
[93] CARRUTHERS J. A. and BIEBER T. J., *Appl. Phys.*, **40** (1969) 426.
[94] HAU L. V., HARRIS S. E., DUTTON Z. and BEHROOZI C. H., *Nature*, **397** (1999) 594.
[95] BIGELOW M. S., LEPESHKIN N. N. and BOYD R. W., *Science*, **301** (2003) 200.
[96] BIGELOW M. S., LEPESHKIN N. N. and BOYD R. W., *Phys. Rev. Lett.*, **90** (2003) 11.
[97] OKAWACHI Y., BIGELOW M. S., SHARPING J. E., ZHU Z., SCHWEINSBERG A., GAUTHIER D. J., BOYD R. W. and GAETA A. L., *Phys. Rev. Lett.*, **94** (2005) 153902.
[98] SCHWEINSBERG A., LEPESHKIN N. N., BIGELOW M. S., BOYD R. W. and JARABO S., *Europhys. Lett.*, **73** (2006) 218.
[99] SONG K. Y., HERR'AEZ M. G. and LUC THEVENAZ, *Opt. Express*, **13** (2005) 82.
[100] OKAWACHI Y., FOSTER M. A., SHARPING J. E., GAETA A. L., XU Q. and LIPSON M., *Opt. Express*, **14** (2006) 2317.
[101] YARIV A., XU Y., LEE R. K. and SCHERER A., *Opt. Lett.*, **24** (1999) 711.

[102] Harris S. E., Field J. E. and Imamoglu A., *Phys. Rev. Lett.*, **64** (1990) 10.
[103] Budker D., Kimball D. F., Rochester S. M. and Yashchuk V. V., *Phys. Rev. Lett.*, **83** (1999) 1767.
[104] Liu C., Dutton Z., Behroozi C. H. and Hau L. V., *Nature*, **409** (2001) 490.
[105] Akulshin A. M., Barreiro S. and Lezama A., *Phys. Rev. Lett.*, **83** (1999) 4277.
[106] Schwarz S. E. and Tan T. Y., *Appl. Phys. Lett.*, **10** (1967) 4.
[107] Hillman L. W., Boyd R. W., Krasinski J. and Stroud C. R. jr., *Opt. Commun.*, **45** (1983) 6.
[108] Fabelinskii I. L., *Molecular Scattering of Light* (Plenum Press, New York) 1968.
[109] Feynman R. P., Leighton R. B. and Sands M., *The Feynman Lectures on Physics*, Vol. **I** (Addison-Wesley, Reading, MA) 1963.
[110] Hellwarth R. W., *Phys. Rev.*, **130** (1963) 1850.
[111] Mandelstam L. I., *Zh. Russ. Fiz. Khim. Ova.*, **58** (1926) 381.
[112] Brillouin L., *Ann. Phys. (Paris)*, **17** (1922) 88.
[113] Gross E., *Nature*, **126** (1930) 400.
[114] Raman C. V., *Indian J. Phys.*, **2** (1930) 387.
[115] Garmire E., Pandarese F. and Townes C. H., *Phys. Rev. Lett.*, **11** (1963) 160.